Conversion of CO_2 into Commercial Materials Using Carbon Feedstocks

Final Report

Reporting Period:
June 1, 2010 to May 31, 2014

by

Jian-Ping Shen, Jonathan Peters, Marty Lail, Paul Mobley, and Brian Turk

DOE Cooperative Agreement No. DE-FE0004329

Submitted by:

Research Triangle Institute
Post Office Box 12194
Research Triangle Park, NC 27709-2194

June 2014

Disclaimer

This report was prepared as an account of work sponsored by an agency of the United States Government. Neither the United States Government nor any agency thereof, nor any of their employees, makes any warranty, express or implied, or assumes any legal liability or responsibility for the accuracy, completeness, or usefulness of any information, apparatus, product, or process disclosed, or represents that its use would not infringe privately owned rights. Reference herein to any specific commercial product, process, or service by trade name, trademark, manufacturer, or otherwise does not necessarily constitute or imply its endorsement, recommendation, or favoring by the United State Government or any agency thereof. The views and opinions of authors expressed therein do not necessarily state or reflect those of the United States Government or any agency thereof.

Abstract

In this project, our research focused on developing reaction chemistry that would support using carbon as a reductant for CO_2 utilization that would permit CO_2 consumption on a scale that would match or exceed anthropomorphic CO_2 generation for energy production from fossil fuels. Armed with the knowledge that reactions attempting to produce compounds with an energy content greater than CO_2 would be thermodynamically challenged and/or require significant amounts of energy, we developed a potential process that utilized a solid carbon source and recycled the carbon to effectively provide infinite time for the carbon to react.

During testing of different carbon sources, we found a wide range of reaction rates. Biomass-derived samples had the most reactivity and coals and petcoke had the lowest. Because we had anticipated this challenge, we recognized that a catalyst would be necessary to improve reaction rates and conversion. From the data analysis of carbon samples, we recognized that alkali metals improved the reaction rate. Through parametric testing of catalyst formulations we were able to increase the reaction rate with petcoke by a factor of >70.

Our efforts to identify the reaction mechanism to assist in improving the catalyst formulation demonstrated that the catalyst was catalyzing the extraction of oxygen from CO_2 and using this extracted oxygen to oxidize carbon. This was a significant discovery in that if we could modify the catalyst formulation to permit controlled the oxidation, we would have a very power selective oxidation process. With selective oxidation, CO_2 utilization could be effective used as one of the process steps in making many of the large volume commodity chemicals that support our modern lifestyles.

The key challenges for incorporating these functionalities into the catalyst formulation were to make the oxidation selective and lower the temperature required for catalytic activity. We identified four catalyst families that had the potential to meet these challenges. Initial screening of the catalyst families did show that the reduction/oxidation activity did occur at lower temperatures and that these catalysts were able to cause carbon chain growth as well as C—C cleavage.

A preliminary techno-economic feasibility of using petcoke/catalyst to produce a CO-rich syngas product was completed and showed significant economic promise. Testing of the different catalyst families demonstrated that Catalyst A was able to stably produce 5 sccm of ethylene/gram of catalyst at 900°C for one hour. For dry methane reforming, our Catalyst 4 was able to achieve production rates of > 10 sccm of CO and > 3 sccm of H_2 per gram of catalyst at 600°C and 350 psig. Based on these developments, the potential for CO_2 utilization in the production of large volume commodity chemicals is very promising.

Table of Contents

Abstract iii
1. Executive Summary 1
2. Introduction 2
3. Carbon Reactivity Testing 3
3.1 Carbon Sources 3
3.2 Composition Effects 5
3.3 Operating Conditions 7
4. Catalyst Synthesis, Characterization, and Screening 9
4.1 Initial Catalyst Screening Tests 9
4.2 Evaluation of Potential Supports 10
4.3 Investigation of ZnO's catalytic activity 11
4.4 Promoter Evaluation 13
4.5 Parametric Testing of Catalyst Formulations 14
4.6 Preparation of Spray-Dried Catalyst Formulations 18
4.7 Parametric Reaction Testing 19
4.7.1 Effect of CO_2 Concentration 19
4.7.2 Effect of Weight Hourly Space Velocity (WHSV) 19
4.7.3 Effect of CO on Reaction Rate 20
4.7.4 Effect of Catalyst Pre-reduction on CO Production 20
4.7.5 Use of Controlled Carbon Species to Investigate Catalytic Reaction Mechanism 22
4.7.2 Effect of Catalyst /Carbon Contact 22
5. Reaction Mechanism Investigation 23
5.1 Thermogravimetric Testing 23
5.2 Autochem Testing 25
5.3 Bench-scale Testing 28
6. Evaluation of Potential Chemical Intermediates 29
7. Process Economics of CO_2 Utilization for Syngas Production 32
8. Catalyst Development for Direct Chemical Conversion 35
8.1 Catalysts screening 36
8.2 Ethylene Production 41
8.3 Dry Reforming of Methane 42
9. Conclusions 45
10. References 47

List of Figures

Figure 1. Bench-scale fluidized testing system 3
Figure 2. The char reactivity under the reaction conditions of WHSV= 2.36 h^{-1}, P=1 atm, and T=800°C 5
Figure 3. The correlation between char reactivity and its oxygen content 6
Figure 4. The switchgrass char reactivity collected at 700°C, WHSV=2.36 $h^{-}1$, and various pressures 7
Figure 5. The switchgrass char reactivity collected with and without catalyst (K-Ca/SnO-Fe_2O_3 at 700°C, 100 psig and WHSV=2.36 h^{-1} 7
Figure 6. The switchgrass char reactivity collected at various temperatures and WHSV=2.36 h^{-1} 9
Figure 7. The petcoke reactivity with various particle size distributions collected under the reaction conditions of WHSV=2.36 h^{-1}, P=1 atm, and T=800°C 9
Figure 8. The petcoke reactivity collected under the reaction conditions of WHSV=1.18 h^{-1}, T=800°C, and O_2=2% when used 9
Figure 9. The petcoke char reactivity collected over K-Ca based catalysts under the conditions of WHSV=2.36 h^{-1} and T=800°C 11
Figure 10. The catalytic waste tire and switchgrass char reactivities collected under the conditions of WHSV=2.36 h^{-1} and T=800°C 11
Figure 11. The X-ray diffraction patterns of fresh and spent mixture of graphite and K-Ca/ZnO-CeO_2 12
Figure 12. The petcoke char reactivity collected in the presence of K-Ca/ZnO-CeO_2 catalyst with difference Zn/Ce ratio at 800°C and WHSV=2.36 h^{-1} 13
Figure 13. The CO_2 petcoke char gasification reactivity collected over various spray dried catalysts at 800 °C, 1 atm, and WHSV=2.36 h^{-1} 15
Figure 14. The CO_2 petcoke char gasification reactivity collected over various impregnated catalysts at 800 °C, 1 atm, and WHSV=2.36 h^{-1} 15
Figure 15. The CO_2 petcoke char gasification reactivity collected over the catalysts with various K and Mg loadings at 800 °C, 1 atm, and WHSV=2.36 h^{-1} 15
Figure 16. CO_2 petcoke char gasification reactivity collected over the catalysts with various Al_2O_3 contents and fixed loading of K and Mg at reaction conditions of 800 °C, 1 atm, and WHSV=2.36 h^{-1} 17
Figure 17. CO_2 petcoke char gasification reactivity collected over the catalysts with various Al_2O_3 contents and fixed loading of K and Mg at reaction conditions of 800 °C, 1 atm, and WHSV=2.36 h^{-1} 17
Figure 18. CO_2 petcoke char gasification reactivity collected over the catalysts with various Al_2O_3 contents and 10 K loading at reaction conditions of 800 °C, 1 atm, and WHSV=2.36 h^{-1} 18
Figure 19. The catalytic CO_2 petcoke char gasification performances collected over the K-Mg/SnO_2-Fe_2O_3-Al_2O_3 catalysts prepared using different methods at 800°C, and WHSV=2.36 h^{-1} 19
Figure 20. The catalytic petcoke char reactivity collected over the K-Mg/SnO_2-Fe_2O_3-Al_2O_3 catalyst prepared using spray drying method at 800 °C, 1 atm, and WHSV = 2.36 h^{-1} 19
Figure 21. Switchgrass char reactivity during CO_2 gasification collected at 800°C, 1 atm, GHSV=1,000 h^{-1}, and various CO_2 concentrations 20

Figure 22. Switchgrass char reactivity during CO_2 gasification collected at 700 ºC, 1 atm, and various WHSV 20
Figure 23. Switchgrass char reactivity under various feed compositions at 800ºC, and GHSV=1,000 h^{-1} 20
Figure 24. The CO production profiles collected at 800 ºC and 1 atm for CO_2 reduction capability evaluation of two catalysts with and without H_2 pre-reduction 21
Figure 25. The methane dry reforming activity of the K-Mg/SnO_2-Fe_2O_3-Al_2O_3 catalyst collected at 800 ºC and WHSV=2.36 h^{-1} 22
Figure 26. Weight loss profiles during TGA reduction with CO in N_2 and oxidation with CO_2 . 24
Figure 27. Weight loss profiles during TGA oxidation with CO_2 and air 24
Figure 28. Weight loss profiles during TGA reduction and oxidation with air 25
Figure 29. MS profiles during exposure of the catalyst to 20% CO in He while heating from 30ºC to 800ºC 26
Figure 30. MS profiles during exposure of the catalyst to $C^{18}O_2$ while heating from 30ºC to 800ºC 27
Figure 31. MS profiles during exposure of the catalyst to 20% CO in He while heating from 30ºC to 800ºC after exposure to $C^{18}O_2$ 28
Figure 32. Reactor effluent profiles for catalyst and petcoke during heating from 30ºC to 800ºC and after exposure to reduction and exposure to CO_2 29
Figure 33. Results from ranking strategy used to assess most promising chemical intermediates 32
Figure 34. Block Flow Diagram of the CO_2 utilization process 32
Figure 35. Sensitivity analyses of CO_2 utilization process 34
Figure 36. Results from TPR screening of catalyst formulations for the different catalyst families 36
Figure 37. Results from CO_2 oxidation during TGA-MS screening for the different catalyst families 37
Figure 38. Effluent Concentration Profiles for Catalyst D at 600°C at 25 bar with CH_4 and CO_2 38
Figure 39. Effluent Concentration Profiles for Catalyst D at 600°C at 25 bar with CH_4 and CO_2 39
Figure 40. Effluent Product Profile for Catalyst A at 780°C with CH_4 and CO_2 39
Figure 41. Effluent Product Profile for Catalyst A at 700°C with propane and CO_2 40
Figure 42. Effluent ethylene yield profiles vs. time for examined catalysts from 800°C to 900°C at atmospheric pressure with a CH_4 feed 42
Figure 43. Modeled CO yield response surfaces for different catalysts over varying temperature, pressure, and reactant feed ratios 43
Figure 44. Modeled H_2 yield response surfaces for different catalysts over varying temperature, pressure, and reactant feed ratios 44
Figure 45. Modeled CO to H_2 product ratio response surfaces for different catalysts over varying temperature, pressure, and reactant feed ratios 45

List of Tables

Table 1. Carbon source preparation and initial characterization 4
Table 2. Elemental analysis of char samples from XRF measurement 6
Table 3. The catalytic reaction performance under conditions of WHSV=2.36 h^{-1} and T=800°C 10
Table 4. The catalytic reaction performance under conditions of WHSV=2.36 h^{-1} and T=800°C 14
Table 5. The surface area collected over the catalysts with various compositions..... 16
Table 6. Chemical intermediates evaluated with ranking strategy 30
Table 7. Criteria used to quantify project benefits..... 31
Table 8. Criteria used to quantify likelihood of success..... 31
Table 9. Assumptions made during development of cash flow model..... 34
Table 10. Chemical intermediates evaluated with ranking strategy 35

1. Executive Summary

The objective of this project was development of a CO_2 utilization process that used carbon as a reductant and would result in consumption of CO_2 on a large enough scale to match or exceed anthropomorphic CO_2 generation from the use of fossil fuels for energy. Our original goal was production of CO, which is the easiest compound of value to be produced from CO_2. The key challenge for this development effort was achieving sufficient reactivity and conversion of the carbon and CO_2.

Our efforts began with evaluation of the natural reactivity of different carbon sources with CO_2. We tested a wide range of carbon sources which included a series of coals and petcoke, different components of municipal solid waste, and different biomass sources. We found that the different carbon sources had a wide range of reactivity with CO_2 with biomass sources having the highest reactivity and petcoke having the lowest.

Our next step focused on increasing this natural reactivity with catalysts. Our analysis of the different carbon sources to identify a correlation between composition and/or physical properties and reactivity did not yield any valuable and statistically significant correlation. However, a weak relationship between reactivity and alkali metals was noticed. Using this as a starting point, catalyst formulations were prepared. By using parametric testing of catalyst composition, we systematically fine-tuned our catalyst formulation to maximize and stabilize catalytic activity for reactivity between CO_2 and petcoke. Our optimal catalyst formulations were able to improve reactivity of petcoke by a factor of > 70.

While evaluating the reaction mechanism to find new means of increasing reactivity of our catalysts, we were able to demonstrate that the reaction mechanism for our catalyst involved adsorption of CO_2, extraction of oxygen from this adsorbed CO_2 and use of this extracted oxygen for the oxidation of carbon. Our initial investigation showed that this carbon source could be CO or petcoke. The core concept in this discovery was our catalyst was essentially extracting one of the oxygen from CO_2 and using this oxygen for oxidation. If our catalyst could also control the oxidation process, our discovery could be used for selective oxidation. Because CO_2 is a very poor oxidation agent, this catalytic path could provide a very strong and selective oxidation route in what would otherwise be a very poor oxidizing environment. One particular area were this would be extremely valuable is oxidative coupling of methane, but this was just one of many potential opportunities.

To prioritize our research activities, the project team completed a structured evaluation of the potential chemical intermediates based on the perceived market available for the chemical and the likelihood for successful catalyst development based on our current state of development. The results from this evaluation indicated that syngas was our top choice followed by ethylene oxide and methanol. Another result from this evaluation was it identified the key challenges that our current catalyst would have to overcome to exploit selective oxidation. These challenges included:

- Catalytic oxygen extraction activity occurs at temperatures typically higher than used for synthesizing most chemical intermediates.

- Conversion of the raw hydrocarbon into the desired chemical intermediate requires both a very selective and targeted oxidation reaction for yields that would be commercially attractive.
- Selection of the appropriate hydrocarbon feedstock that can be effectively converted into a desirable product by the selective oxidation being catalyzed.

Based on these challenges, we were able to identify four families of catalysts that should be able to overcome these challenges. Our initial testing of these catalyst families did show a reduction in the oxidation/reduction temperature. In preliminary testing with methane, these catalysts also showed evidence of carbon chain growth and C—C cleavage, both of which would be very valuable for direct chemical production with CO_2 utilization. To maintain a focused research approach, we tested our catalyst families for ethylene production to evaluate a carbon chain growth reaction and dry reforming of methane to evaluate C—C cleavage. For ethylene production, our Catalyst D was able to stably produce 5 sccm of ethylene/gram of catalyst at 900°C for one hour. For dry methane reforming, our Catalyst 4 was able to achieve production rates of > 10 sccm of CO and >4 sccm of H_2 per gram of catalyst at 600°C and 350 psig. These results show that our catalyst formulations have the potential to effective use CO_2 as a selective oxidation agent enabling CO_2 utilization on a scale that could match or exceed anthropomorphic CO_2 generation from fossil fuel consumption.

2. Introduction

RTI is developing a novel CO_2 utilization process which converts CO_2 into CO through a reaction with abundant low-value carbon sources. Effectively exploiting plentiful carbon sources, like petcoke, sub-bituminous coal, lignite, and biomass as a carbon reductant can achieve a large impact for CO_2 utilization. In a transport reactor-based CO_2 converter (TRCC), a circulating solids mixture predominantly composed of carbon and catalyst is used to optimize the production of CO from carbon, CO_2, and O_2. This TRCC creates ideal conditions for rapid heat and mass transfer, which facilitates the use of the exothermic heat generated by reaction of O_2 with carbon to drive the endothermic reverse Boudouard reaction, $C + CO_2 \leftrightarrow 2CO$. The catalyst and any unreacted carbon entrained out the reactor with the CO-rich product gas are separated and returned to the inlet of the transport reactor. The combination of rapid heat and mass transfer and recycle of unreacted carbon allows the TRCC to achieve higher productivity of desired product(s). Because transport reactors maximize throughput based on both reactor size and footprint, the TRCC can reduce reactor system cost and make this process competitively attractive.

In this project, the technical feasibility of the proposed chemistry was evaluated using fluidized bed and thermogravimetric (TGA) tests to investigate carbon/CO_2 reactivity and screen catalysts for enhancing carbon/CO_2 reactivity for both renewable- and fossil-based carbon sources. Process simulation and modeling are being used to evaluate different process configurations for optimizing CO_2 conversion and evaluating process economics. RTI also evaluated options of producing other chemicals that meet DOE/NETL's cost goal of $10/ton of CO_2.

3. Carbon Reactivity Testing

3.1 Carbon Sources

A variety of carbon samples obtained through pyrolysis of biomass and fossil fuels were prepared and tested for reactivity toward CO_2 conversion using the modified bench-scale fluidized bed reactor system, shown in Figure 1. Table 1 summarizes the temperature conditions of the pyrolysis process used to produce the char; the char yield; and the carbon, hydrogen, and nitrogen elemental analysis for the char samples. The pyrolysis temperatures used for the biomass samples were at the upper end of the temperature range typically being used for biomass pyrolysis processes. Higher temperatures were used for the coal pyrolysis because of the lower reactivity of coal**.**

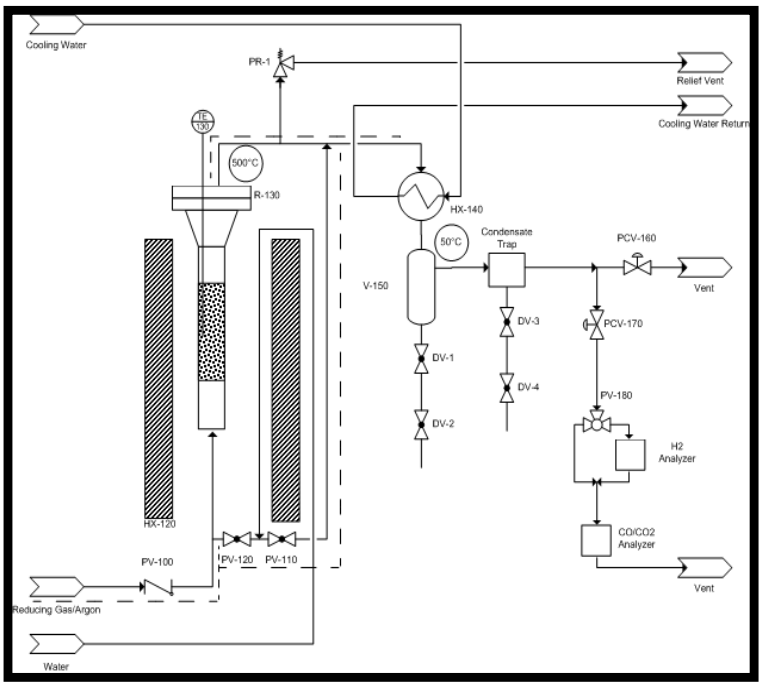

Figure 1. Bench-scale fluidized testing system

In order to compare the inherent reactivity of different carbon and char samples on the same basis, the weight hourly space velocity (WHSV) defined in Equation 1 was kept the same during all the tests.

$$\text{WHSV } (h^{-1}) = \frac{F_{CO_2}/22.414 \times 44}{W_{char}} \quad (1)$$

In Equation 1, F_{CO2} represents the volumetric flow rate of CO_2 in standard liters per minute (slpm) and W stands for the initial mass of sample loaded in grams. Figure 2 shows the sample reactivity in term of maximal CO production rate defined in Equation 2, where $F_{CO,m}$ represents the maximal volumetric flow rate of CO produced in slpm and W_0 stands for the initial mass of loaded sample in grams.

$$r_{CO,m} \ (\text{min}^{-1} \times 10^3) = \frac{F_{CO,m}/22.414 \times 28}{W_0} \quad (2)$$

Table 1. Carbon source preparation and initial characterization

Carbon source		Char Preparation		Elemental Analysis (wt%)				Surface Area (m^2/g)
		Temperature (°C)	Yield (wt%)	C	H	N	O	
Fossil fuel	Petcoke char	800	92.5	94.8	0.5	1.0	0	3.2
	Bituminous coal char	800	52.6	85.9	0.6	1.3	0.6	0.7
	Sub-bituminous coal char	800	43.3	83.4	0.5	0.5	0.7	116.3
	Lignite coal char	800	34.4	75.0	2.1	0.5	5.6	5.6
Biomass	Wheat straw char	500	22.1	97.9	2.2	0.0	3.5	19.0
	Pine char	500	22.5	87.7	2.6	0.0	3.1	278.5
	Corn stover lignin char	500	38.5	87.2	2.3	1.7	3.3	11.7
	White oak char	500	6.1	68.0	3.1	0.0	10.4	2.6
	Switchgrass char	500	18.3	60.4	3.6	0.2	11.5	3.4
	Corn stover char	500	23.4	53.7	2.7	0.0	8.5	2.1
	Rice husk char	500	35.2	45.4	1.6	0.8	1.6	214.2
	Bamboo char	800	13.1	79.4	0.7	1.6	5.6	3.1
	Kudzu vine char	800	21.7	78.6	0.6	1.2	4.8	3.3
	Kelp char	800	32.3	62.6	1.0	1.6	16.9	62.6
Municipal waste	Waste tire char	800	34.3	83.1	0.4	0.3	0	75.9
	Food scraps char	800	14.1	77.5	1.0	2.7	7.3	1.8
	Waste plastic char	800	13.4	90.4	0.7	0	0.2	411.7
	Waste paper char	800	21.3	64.7	0.8	0	0	208.6
	Sewage sludge char	800	30.1	36.3	0.7	2.4	6.2	33.5

Carbon reactivity for CO_2 conversion for the samples tested varies based on carbon source ranging from a low of 0.38 x 10^{-3} min^{-1} for petcoke char to a high of 29.46 x 10^{-3} min^{-1} for switchgrass char. Chars generated from carbon sources derived from municipal solids wastes and biomass tend to be more reactive. Char samples generated from carbon sources composed of primarily carbon with less than 1.0% of hydrogen, nitrogen, and oxygen, like petcoke, bituminous coal, and waste tires, had low reactivity. The reactivity for low rank coal sources (sub bituminous coal and lignite) was essentially identical to the least reactive biomass and municipal solid waste carbon samples. Based on this information, low rank coals, biomass and municipal solid waste represent promising carbon sources for CO_2 gasification to generate CO while consuming CO_2. Low rank coals have the additional advantage of being available in large quantities and at a cost that encourages economies of scale.

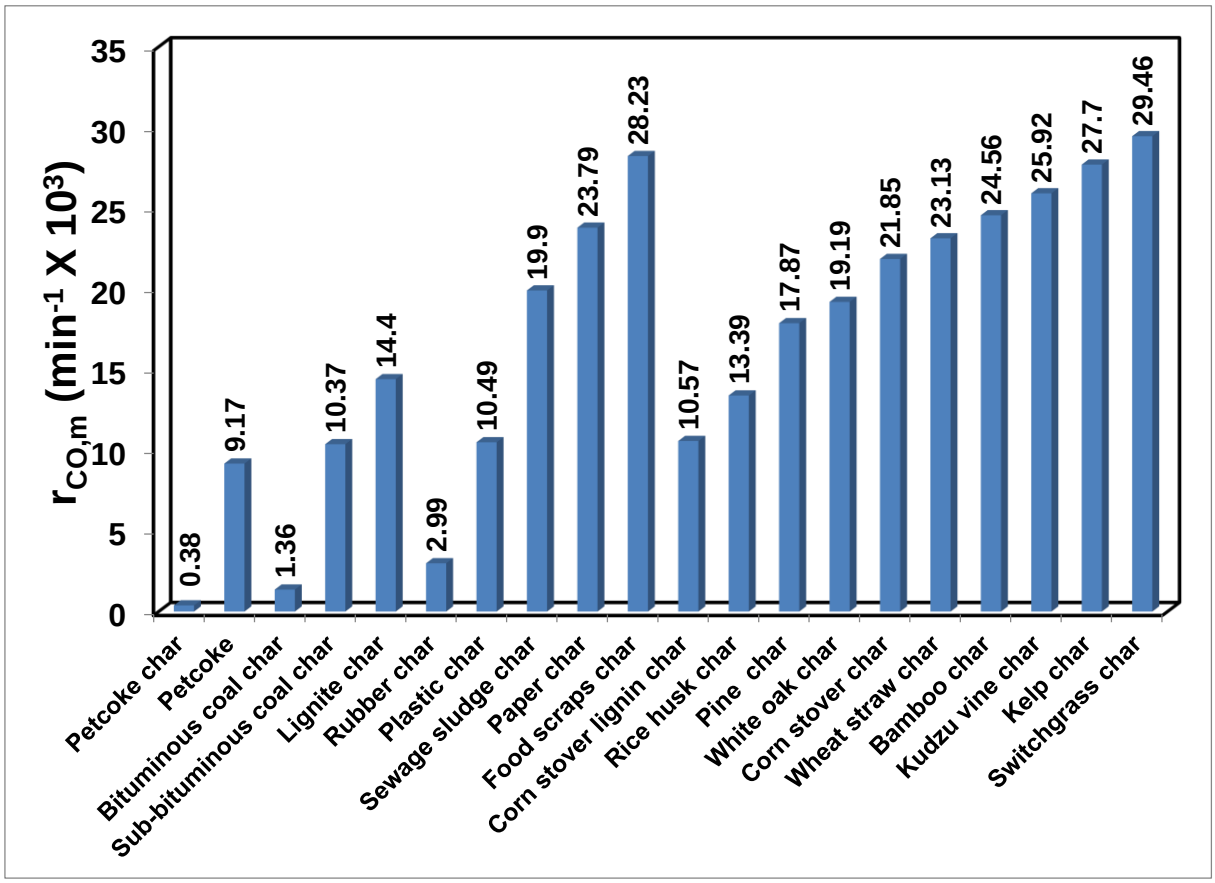

Figure 2. The char reactivity under the reaction conditions of WHSV= 2.36 h^{-1}, P=1 atm, and T=800°C

3.2 *Composition Effects*

Because the chars used for reactivity testing were generated from carbon sources with very diverse properties, an attempt was made to identify correlations between char properties and reactivity. For the properties listed in Table 1, the strongest correlation with reactivity was with oxygen content. Figure 3 shows the correlation between reactivity and oxygen content of the carbon sources tested. Although Figure 3 does show a correlation between reactivity and oxygen content, this correlation is not especially reliable for predicting reactivity from the oxygen content of a carbon source. One factor not present in Table 1 that might result in stronger correlation with reactivity is the mineral content of the carbon source. Samples of the carbon sources were submitted for mineral analysis using an X-Ray Fluorescence (XRF) technique to collect the necessary data to evaluate any correlations between mineral content and reactivity. Table 2 provides the results from this analysis.

The results in Table 2 support the common observation that biomass and biomass-derived carbon sources have high alkali (e.g., K) metal concentrations. These high alkali concentrations are also generally believed to promote higher activity for biomass and biomass-derived samples, because alkali metals are known their catalytic activity for carbon gasification. Although the results in Table 2 support this hypothesis, the alkali metal concentrations in the samples do not directly correlate with observed CO production rate. No other specific correlations between the elemental concentrations and reactivity of the carbon source were identified.

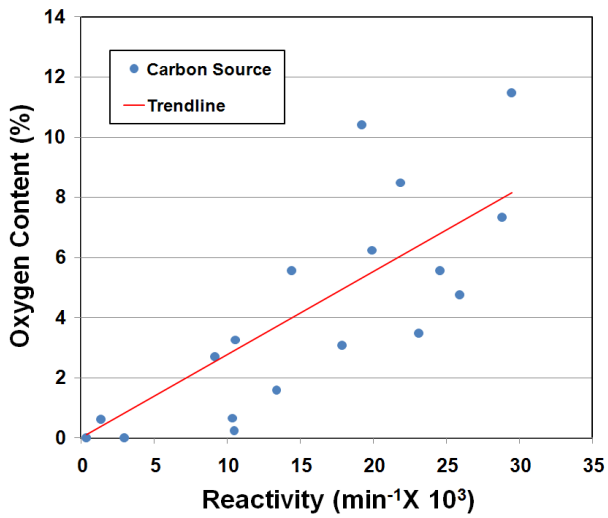

Figure 3. The correlation between char reactivity and its oxygen content

Table 2. Elemental analysis of char samples from XRF measurement

Carbon source		Elemental Analysis (wt%)									
		Mg	Al	Si	P	S	Cl	K	Ca	Ti	Fe
Fossil fuel	Petcoke char	BQL	0.44	0.46	BQL	2.14	BQL	0.03	0.05	0.06	0.27
	Bituminous coal char	0.14	1.58	3.08	BQL	2.93	BQL	0.22	0.66	0.08	2.80
	Sub-bituminous char	0.65	2.07	2.73	0.14	0.87	BQL	0.10	5.57	0.33	2.17
	Lignite coal char	0.28	2.54	3.53	0.30	0.78	BQL	0.17	6.29	0.37	2.24
Biomass	Wheat straw char	0.45	0.20	0.86	0.65	0.24	0.06	2.72	1.12	0.01	0.06
	Pine char	0.67	0.64	0.26	0.29	0.19	BQL	1.98	2.17	BQL	0.13
	Corn stover lignin char	0.32	0.61	BQL	0.22	0.49	BQL	0.61	0.68	BQL	2.39
	White oak char	0.14	1.32	2.48	0.32	0.22	0.25	7.65	5.38	0.05	0.55
	Switchgrass char	0.68	0.92	2.32	1.38	0.39	1.80	12.6	3.83	BQL	0.25
	Corn stover char	0.25	1.90	12.0	1.08	0.35	1.19	14.3	2.97	0.08	0.85
	Rice husk char	0.33	1.23	44.9	0.76	0.32	BQL	1.97	0.57	BQL	0.22
	Kudzu vine char	1.29	0.15	1.14	1.35	0.33	BQL	3.74	6.44	0.03	0.18
	Kelp char	1.47	0.80	0.25	0.53	9.19	13.1	12.7	8.04	0.24	0.40
Municipal waste	Waste tire char	0.13	0.91	2.67	0.45	5.15	BQL	0.19	0.61	BQL	0.26
	Food scraps char	0.16	0.59	0.06	2.12	0.26	4.82	1.01	2.19	0.02	0.07
	Waste paper char	0.44	10.8	13.4	0.13	0.60	BQL	0.25	6.94	1.00	0.68
	Sewage sludge char	1.81	2.99	6.44	14.4	0.31	BQL	2.34	6.33	0.83	18.1

*BQL: Below Quantitation Limit

3.3 *Operating Conditions*

Thermodynamic equilibrium constraints for the carbon gasification reaction for our process indicate that higher operating pressures will result in lower conversion. However, if the reaction is kinetically controlled, there is the potential that higher operating pressures can be used to enhance reactivity and potentially reduce equipment size at the same throughput. The original safety protocol for our testing system limited operation to atmospheric pressure, because of the pressure limitations for the materials used in the testing system at our typical operating temperatures. To enable investigating the potential effects of pressure on the reaction, the testing system and safety protocol for this testing system were modified to permit operation at system pressures of 100 psig at 800°C.

Figure 4 shows the reactivity of switchgrass char at three different operating pressures. The results show that char reactivity increases with pressure up to 100 psig. These results confirm that the carbon gasification reaction is kinetically controlled. Similar observations have been reported by D. G. Roberts, et al. (2000). Additional testing with a catalyst shown in Figure 5 indicates that although the addition of one of our leading catalysts speeds up the reaction, the reaction rate remains kinetically controlled. Based on the mass of sample loaded in the reactor and spent sample removed from the reactor, carbon consumption during the pressure test was approximately double that observed during the atmospheric test.

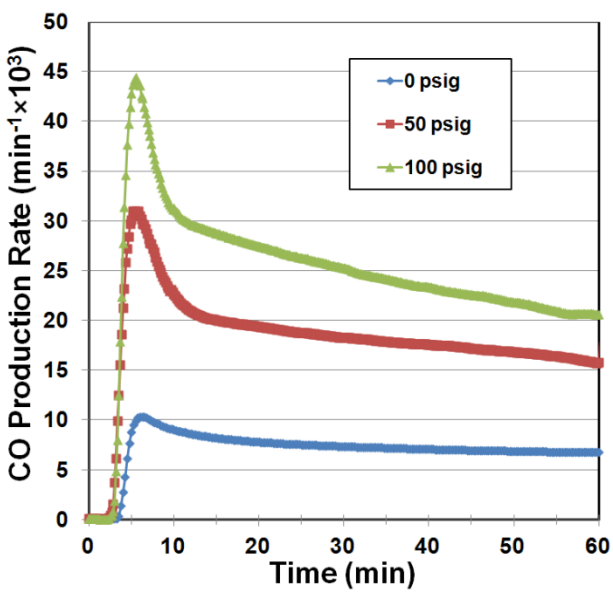

Figure 4. The switchgrass char reactivity collected at 700°C, WHSV=2.36 h-1, and various pressures

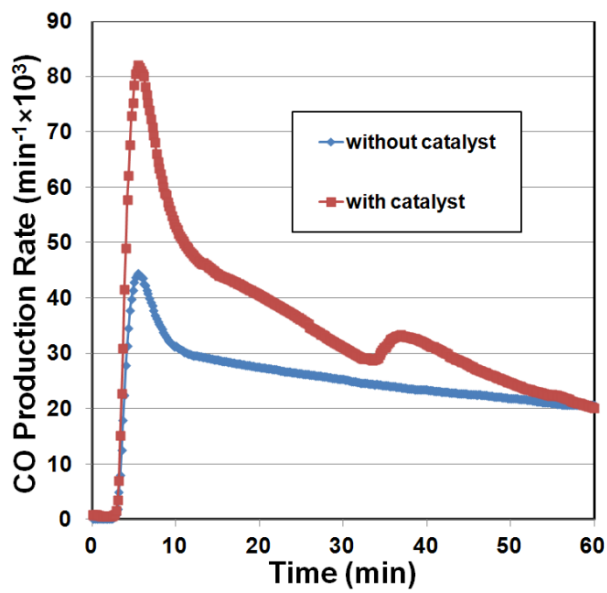

Figure 5. The switchgrass char reactivity collected with and without catalyst (K-Ca/SnO-Fe_2O_3 at 700°C, 100 psig and WHSV=2.36 h^{-1}

The CO production rates for the switchgrass char obtained during a parametric study of the effect of temperature from 600 °C to 900 °C are shown in Figure 6. The CO production rate for the swithchgrass char increases by a factor of about 5 across the temperature range tested. At 900 °C, the measured CO_2 reactivity was 0.047 min^{-1}, which corresponds to about 95% of the reaction rate necessary for 100% conversion of the CO_2. During previous testing of carbon samples, the reactivity with CO_2 dropped by roughly a factor of 10 when the reaction temperature decreased from 900 °C to 800 °C. For the switchgrass char, a decrease in reactivity of roughly a factor of 10 was observed after the reaction temperature decreased from 900 °C to 600 °C. The higher

than anticipated reactivity of the switchgrass char would suggest that the ash components contain materials that catalytically enhance the reactivity of the char with CO_2 even at 600 °C.

The influence of particle size of carbon source was also investigated. The available petcoke was screened to give samples with petcoke particles in four size ranges:

- < 45 µm
- Between 45 µm and 75 µm
- Between 75 µm and 125 µm
- > 125 µm).

The CO production profiles in Figure 7 show that the general CO production profiles all have the same general shape regardless of the carbon sample's particle size. These CO production profiles consist of an initial period of very high reactivity that decreases to a more stable and consistent rate. The maximum CO production rate observed near the start of the reaction (< 15 minutes of reaction) appears to decrease and shift to shorter reaction times with smaller particle size. However, the stable CO production rate for the last 40 minutes of the test increases as the particle size decreases. The reasons for these results are not currently understood.

The reverse Boudouard reaction ($CO_2 + C \leftrightarrow 2CO$) is an endothermic reaction. To provide the energy necessary to drive this endothermic reaction and maintain the necessary reaction temperature, oxygen will be co-fed with CO_2 to provide the required energy through partial oxidation of carbon to CO. Because complete oxidation of the carbon would produce CO_2, which is counterproductive, a test with petcoke was conducted to determine the relative reaction rates for oxidation and the reverse Boudouard reaction. The CO and CO_2 profiles for this test and the base case without O_2 addition are shown in Figure 8. Based on the differences in the CO_2 and CO profiles, a small amount of the CO product was reacting with O_2 to form CO_2 in the test in which CO_2 and O_2 are co-fed to the reactor. This would indicate that second reaction step for full combustion ($CO + 0.5\ O_2 = CO_2$) is slightly faster than the reverse Boudouard reaction at 800 °C. This is a very promising as the results from the parametric temperature testing show that the reaction rate for the reverse Boudouard reaction significantly increases at 900 °C. Considering that this test was conducted with petcoke, one of the least reactive carbon sources, these results demonstrate the technical feasibility of the fundamental premise of our process that co-feeding CO_2 and O_2 with carbon at high temperatures can result in the net conversion of CO_2 into CO.

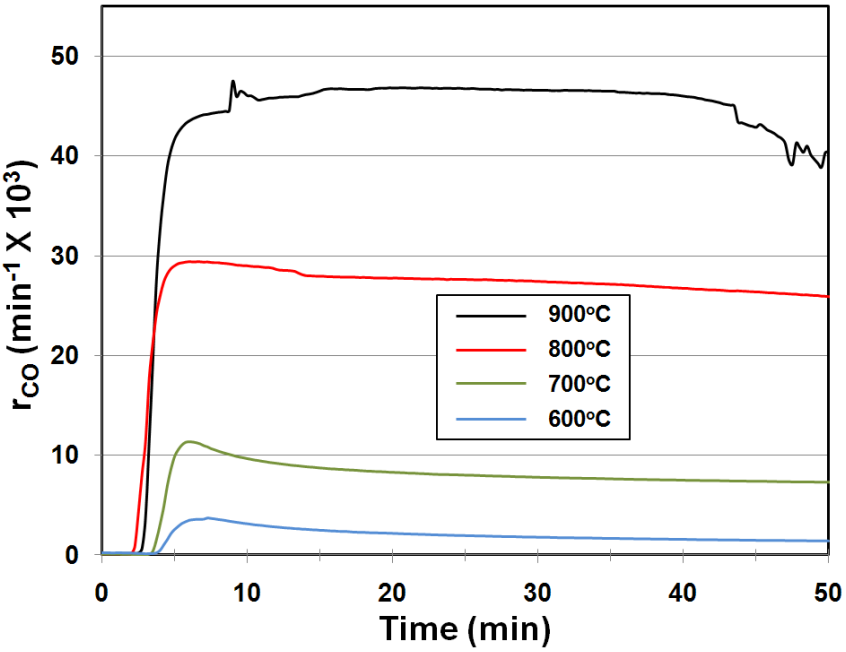

Figure 6. The switchgrass char reactivity collected at various temperatures and WHSV=2.36 h^{-1}

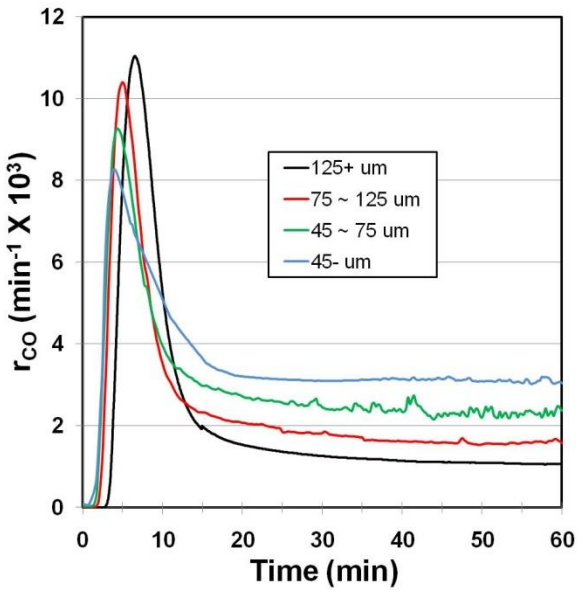

Figure 7. The petcoke reactivity with various particle size distributions collected under the reaction conditions of WHSV=2.36 h^{-1}, P=1 atm, and T=800°C

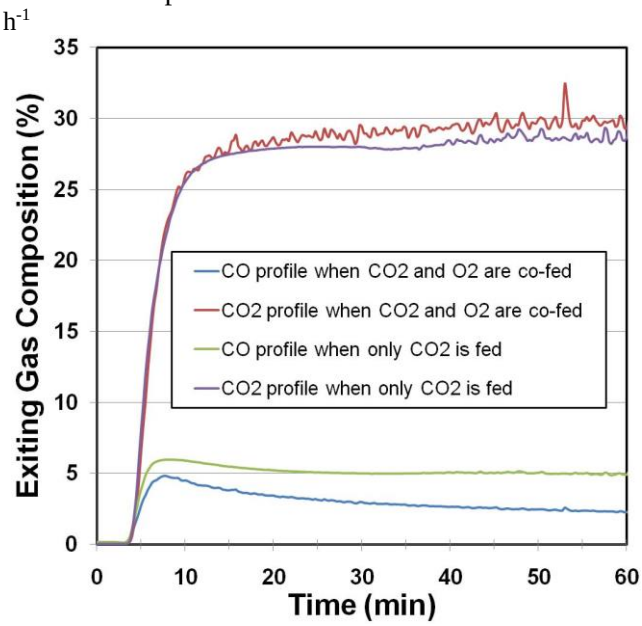

Figure 8. The petcoke reactivity collected under the reaction conditions of WHSV=1.18 h^{-1}, T=800°C, and O_2=2% when used

4. Catalyst Synthesis, Characterization, and Screening

4.1 Initial Catalyst Screening Tests

The effect of prepared catalysts on carbon feedstock/CO_2 reactivity was evaluated in our fluidized-bed reactor system. Test samples consisted of homogeneous mixtures composed of 4:1

mass ratio of catalyst to carbon. Petcoke was chosen as the carbon feedstock for the screening activities because it has the lowest reactivity with CO_2 and should have the greatest potential to demonstrate catalytic activity. The catalyst reactivity was calculated using the same principles used for evaluating carbon reactivity described in Section 2.1. The results from screening an initial set of catalysts is provided in Table 3.

In Table 3, the catalyst samples that contain both alkali and alkali earth metals (K-Ca and K-Mg) demonstrated some of the highest activities of the initial set of catalysts tested. All catalyst samples with potassium had very high activity demonstrating that this alkali metal is an important active ingredient. In general, catalyst formulations that included transition metals were less active. The addition of cerium, which could possibly act as an oxygen donor to facilitate the CO_2 conversion reaction, did not seem to increase activity as much as the alkali and alkali earth metal combination.

The net outcome of this effort has been to demonstrate that the most active catalyst formulations that have been identified cannot be readily or easily adapted for impregnation onto the carbon source. Thus, the results we have obtained with simple physical mixing of the catalysts and carbon sources represent the best means of contacting the catalyst and carbon sources. With supported catalysts, recovery of the catalyst from the char/ash should be more effective and enable significant reuse of the catalyst. Based on our limited success with attempts to impregnate the carbon source with catalyst, no further work was planned for impregnation of carbon with catalyst.

Table 3. The catalytic reaction performance under conditions of WHSV=2.36 h^{-1} and T=800°C

Catalyst	Reactivity	
	$r_{CO,\,m}$ (min^{-1} x 10^3)	CO_2 conversion (%)
K-Mg/Al_2O_3	19.15	38.32
K-Ca/Al_2O_3	12.34	24.70
Co-Ce/Al_2O_3	11.29	22.59
K/Al_2O_3	9.43	18.87
Pb-Ce/Al_2O_3	8.24	16.49
Cu-Ce/Al_2O_3	7.95	15.91
Fe-Ce/Al_2O_3	5.13	10.26
Sb-Ce/Al_2O_3	4.55	9.10
Mo-Ce/Al_2O_3	2.19	4.39
Zn-Ce/Al_2O_3	1.86	3.73

4.2 Evaluation of Potential Supports

The previous screening tests have demonstrated that a combination of alkali and alkali earth oxides are the most promising active ingredients for a catalyst formulation. The two most promising combination are K-Ca and K-Mg. Based on these active materials, catalyst development has been expanded to include evaluation of support materials for these active components. Our initial support material selection includes Al_2O_3, TiO_2, ZrO_2, CeO_2, and ZnO.

Test results for catalyst combinations of the K-Ca active component and different support materials are shown in Figure 9. Figure 9 clearly shows that the selection of support material can have a significant impact on char reactivity with petcoke char, one of the least reactive carbon sources tested. In Figure 9, the most reactive catalyst combination was K-Ca and ZnO. Testing of this catalyst combination with other char samples, shown in Figure 10, demonstrates that this catalyst combination is effective in increasing reactivity for low reactivity char samples like petcoke and tire wastes chars as well as reactive chars like switchgrass char at temperatures as low as 800ºC.

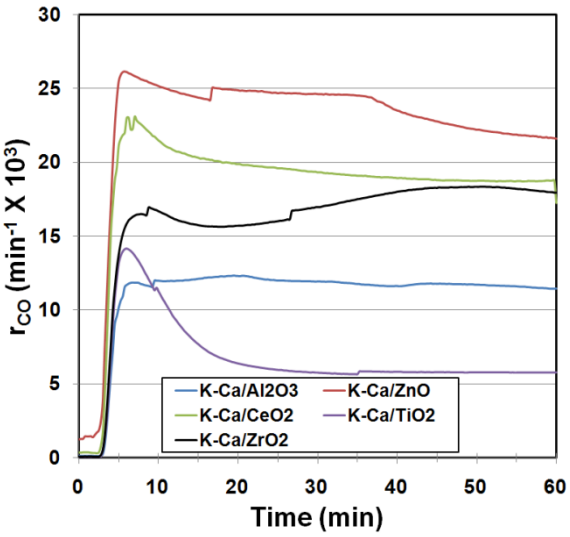

Figure 9. The petcoke char reactivity collected over K-Ca based catalysts under the conditions of WHSV=2.36 h^{-1} and T=800ºC

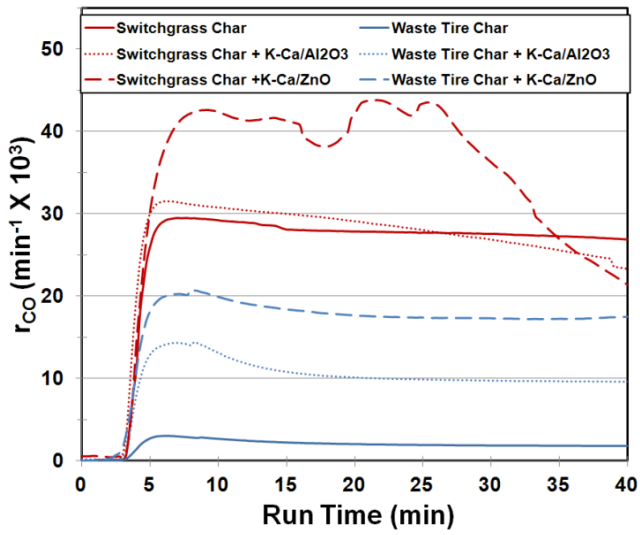

Figure 10. The catalytic waste tire and switchgrass char reactivities collected under the conditions of WHSV=2.36 h^{-1} and T=800ºC

4.3 Investigation of ZnO's catalytic activity

The addition of these support materials was expected to improve mechanical strength of the catalyst and stability of the active components against sintering, fouling, and poisoning, but the catalyst formulations with ZnO resulted in a significantly higher activity and conversion. These results for the ZnO catalyst formulations suggested that the ZnO was acting more like an active component than support.

To explore transformations in the chemical composition of the catalyst during the carbon gasification reaction, XRD analysis was used to examine the crystalline structure of the catalyst material before and after testing. To simplify analysis of the results, graphite, a pure crystalline carbon material, was selected as the carbon source. The selection of graphite for the carbon source facilitated observation of chemical transformations caused by the CO_2 gasification reaction as opposed to chemical interactions with trace chemical species present in other potential carbon sources.

The results for before and after testing of a ZnO/CeO_2 catalyst formulation with high activity and stability are shown in Figure 11. The before and after diffraction patterns have been superimposed in Figure 11 to permit better comparison of the transformations in the crystalline structure of the catalyst during reaction. Because changes in the graphite crystals are not as

important as those in the actual catalyst, Figure 11 was assembled to maximize information about the catalyst crystalline structure and not the graphite crystalline structure.

Figure 11 shows that the two major crystalline species present in the fresh catalyst sample are ZnO and CeO_2 as would be expected. In addition to these major species, there is a very small amount of CaO and $Ca(OH)_2$, which was probably introduced as an impurity during catalyst preparation. In the diffraction pattern for the post test or spent catalyst sample, the results show that the peak intensities for CeO_2 are similar or slightly larger for the spent sample indicating that the amount of this material has not changed during the reaction. By contrast, a significant decrease in the intensity of the ZnO peaks is observed in the spent catalyst sample indicating that crystalline ZnO was being transformed into something else. Because XRD patterns are generated by the ordered structure in crystals, XRD cannot provide information about any non-crystalline phases. The fact that another Zn-based crystalline phase was not present in the spent catalyst sample means that the ZnO was being transformed into an amorphous Zn species or being removed from the catalyst. One potential explanation for the increased carbon gasification activity and the loss of the ZnO crystalline phase was the reduction of ZnO by carbon and subsequent evaporation of the metallic zinc.

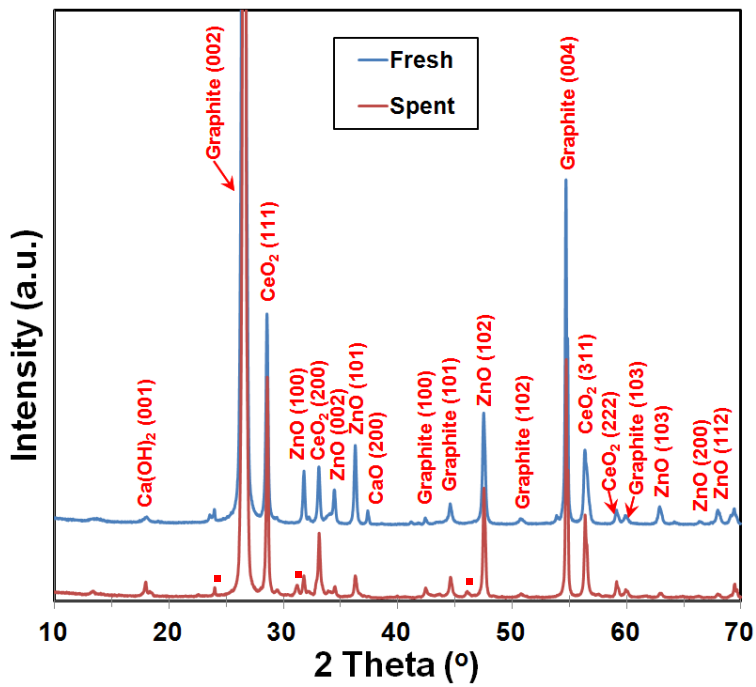

Figure 11. The X-ray diffraction patterns of fresh and spent mixture of graphite and K-Ca/ZnO-CeO_2

Although the reduction of ZnO might increase reactivity, this benefit comes at a gradual consumption of the active ZnO species and loss of Zn through vaporization. A solution to this would be to retain the zinc on the catalyst and effectively reoxidize the zinc into ZnO. Because the addition of CeO_2 did improve the stability of catalyst activity, the XRD patterns were reexamined to identify potential transformations of the CeO_2 that might be impacting zinc species. The XRD pattern for the spent catalyst does include the appearance of a new crystalline phase. The peaks for this new phase are marked with the red squares in Figure 11 and match the diffraction pattern for cerium carbonate. At this time, it is not known if the cerium carbonate was the means by which CeO_2 stabilize the ZnO or just a normal transformation that occured for CeO_2 at our standard test conditions.

During our reexamination of the diffraction patterns for the spent sample, another observation was that CaO present in the fresh sample was not found in the spent sample. However, the intensity of the $Ca(OH)_2$ peak increased. This suggests that at test conditions CaO was converted to $Ca(OH)_2$. As this transformation results from the reaction with water, potential impacts and/or causes for this transformation during the carbon gasification reaction are not known at this time.

To complement the results obtained from XRD analysis, XRF analysis was used to conduct elemental analysis of the fresh and spent ZnO/CeO_2 catalyst samples. The results show that the Zn/Ce ratio decreased from 1.44 in the fresh catalyst sample to 0.43 in the spent catalyst sample. The decrease in the Zn/Ce ratio in the spent catalyst confirms that crystalline ZnO in the fresh catalyst was being consumed during the CO_2 gasification reaction and effectively depleted from the catalyst presumably as metallic zinc vapor. As the Zn/Ce ratio for the spent catalyst was 0.43, an additional catalyst formulation was made with the goal of preparing a fresh catalyst sample with a Zn/Ce ratio of about 0.4 to 0.6. The objective was to investigate if the CeO_2 could stabilize the catalytic activity of ZnO at this ratio. The result of this effort was a fresh catalyst sample with a Zn/Ce ratio of 0.68.

Figure 12 shows the CO production profile for catalyst samples with Zn/Ce ratios of the fresh catalyst of 1.44 and 0.68. The interesting observation in Figure 12 was that the reactivity of these catalysts is essentially identical. Two significant differences were that the catalyst with the higher Zn/Ce ratio had a higher initial peak of CO production at the start of the test and began to show signs of decreasing activity at the end of the test. These observations tended to suggest that the excess ZnO that was apparently reduced and lost as zinc vapor was not responsible for most of the catalytic activity. The presence of the CeO_2 enabled stable CO production for an entire 60 minutes. From XRF analysis of this new catalyst sample, the Zn/Ce ratio decreased from 0.68 in fresh catalyst to 0.47 in spent catalyst. This provided additional evidence that a catalyst with a Zn/Ce ratio of < 0.5 should have increased activity stability.

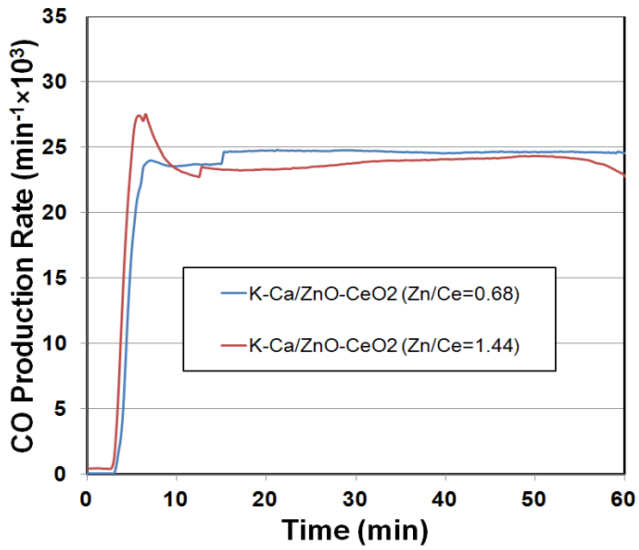

Figure 12. The petcoke char reactivity collected in the presence of K-Ca/ZnO-CeO_2 catalyst with difference Zn/Ce ratio at 800°C and WHSV=2.36 h^{-1}

4.4 Promoter Evaluation

The knowledge gained from attempting to understand the cause for the activity increase for carbon gasification resulting from the use of ZnO and promoters like CeO_2 resulted in many potential combinations for new catalyst formulations. The initial screening results from these new catalyst formulations are shown in Table 4. The values in Table 4 provide activity (maximal CO production rate and corresponding CO_2 conversion) toward CO_2 conversion using petcoke char as carbon source.

A significant number of these new catalyst formulations have consistently shown high reactivity and conversion. One of the key components in these samples was tin oxide that was believed to be providing catalytic activity by a similar mechanism to the ZnO. In general, the effect of the different promoters tested was smaller.

Table 4. The catalytic reaction performance under conditions of WHSV=2.36 h^{-1} and T=800°C

Catalyst	Reactivity	
	$r_{CO,m}$ (min^{-1} x 10^3)	CO_2 conversion (%)
K-Ca/ZnO-CeO_2	27.5	55.0
K-Ca/SnO_2-Fe_2O_3	28.8	57.5
K-Mg/SnO_2-Fe_2O_3	28.2	56.5
K-Mg/ SnO_2-Fe_2O_3-$ZnAl_2O_4$	28.2	56.5
K-Mg/ SnO_2-Fe_2O_3-Al_2O_3	29.1	58.3
K-Ca/SnO_2-CeO_2	25.6	51.2
K-Mg/SnO_2-CeO_2	27.9	55.8
K-Ca/SnO_2-Fe_2O_3-ZnO	29.0	58.0
K-Mg/SnO_2-Fe_2O_3-ZnO	26.0	52.1
K-Mg/SnO_2-Fe_2O_3-ZnO-CeO_2	26.1	52.3
K-Ca/Bi_2O_3	19.9	39.7
K-Mg/Fe_2O_3	26.9	53.7
K-Mg/ Ga_2O_3-Fe_2O_3-Al_2O_3	18.8	37.7
K-Mg/ PbO-Fe_2O_3-Al_2O_3	21.1	42.2
K-Mg/ CuO-Fe_2O_3-Al_2O_3	22.4	44.9
K-Mg/ SnO_2-Fe_2O_3-FCC	23.6	47.2

4.5 Parametric Testing of Catalyst Formulations

Parametric testing focused on our K-Mg/SnO_2-Fe_2O_3-Al_2O_3 catalyst which was our most promising catalyst material. Our initial parametric testing tested different catalyst formulations with and without K and Mg and were prepared as spray dried formulations. The results from this parametric test are shown in Figure 13. Figure 13 shows that the combination of both K and Mg was required to maximize and stabilize the CO production rate. The addition of just K did significantly increase the CO production rate, but this high CO production rate could not be maintained. The catalyst with just Mg inhibited the CO production rate. XRD diffraction patterns showed that the Mg was present as $MgAl_2O_4$ in the final catalyst material.

In a second set of parametric testes, the catalyst formulations were prepared with and without Fe_2O_3, SnO_2, and Al_2O_3 using our previous impregnation preparation procedure. The results from this test are provided in Figure 14. As primary catalytic components, both Fe_2O_3 and SnO_2 demonstrated the ability to catalyze CO production. Furimsky et. al. (1988) and Koama et. al. (1998) have also discussed the role of Fe_2O_3 as an active chemical species and its effect on catalytic performance. However, CO production for the catalyst with a combination of Fe_2O_3 and SnO_2 is only slightly better than Fe_2O_3 catalyst formulation.

The addition of Al_2O_3 also resulted in only a slight increase in the CO production over the other catalyst formulations. However, unlike the previous components, Al_2O_3 was being added

primarily as a support material to provide strength and mechanical integrity. Thus success of the Al_2O_3 in this function was demonstrated by the fact that in spite of the addition of about 40 wt% of Al_2O_3, the CO production increased slightly and appeared to result in a slower loss of CO production through deactivation over the 60 minute test. These performance improvements probably resulted from Al_2O_3 providing an inert support that enables in a stable dispersion of the active catalytic components.

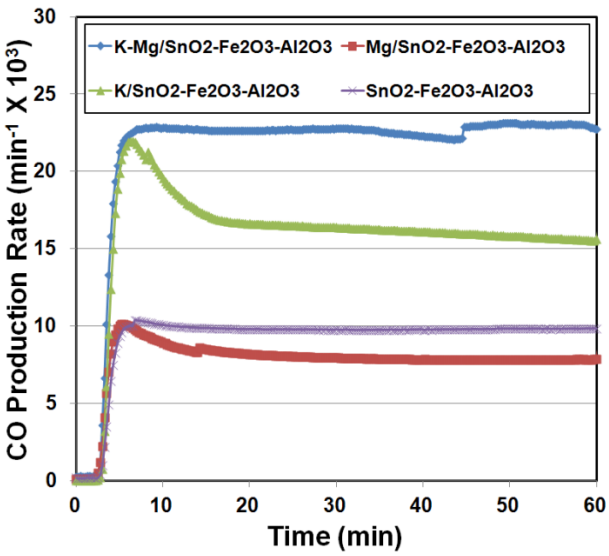

Figure 13. The CO_2 petcoke char gasification reactivity collected over various spray dried catalysts at 800 °C, 1 atm, and WHSV=2.36 h^{-1}

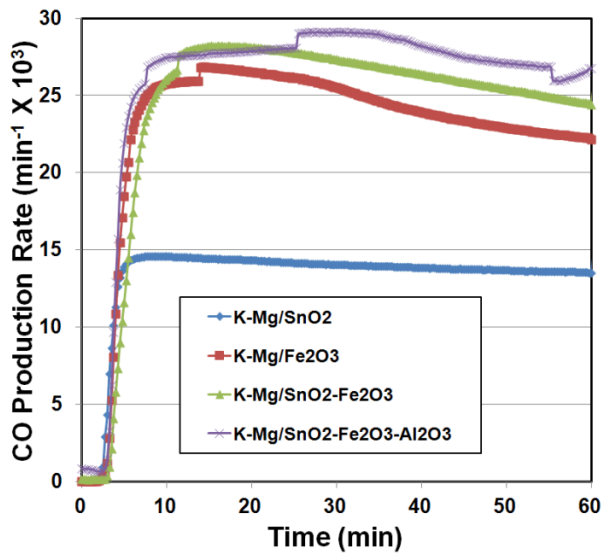

Figure 14. The CO_2 petcoke char gasification reactivity collected over various impregnated catalysts at 800 °C, 1 atm, and WHSV=2.36 h^{-1}

Because our initial parametric test indicated that the combination of K and Mg was necessary for optimal catalyst performance, our parametric tests investigated catalyst formulations prepared with concentrations of 5%, 10%, and 15% of each of these components. The tests results from these catalyst formulations are shown in Figure 15. Figure 15 shows that as the concentration of K and Mg increase, the CO production also increases. At 5% and 10% addition, the CO production rate remained constant for the duration of the test. For the catalyst with 15% addition, CO production did increase, but over the test, the CO production rate declined reaching roughly the same rate observed for the catalyst with 10% addition. Based on these results the optimum addition of K and Mg appears to be near 10%.

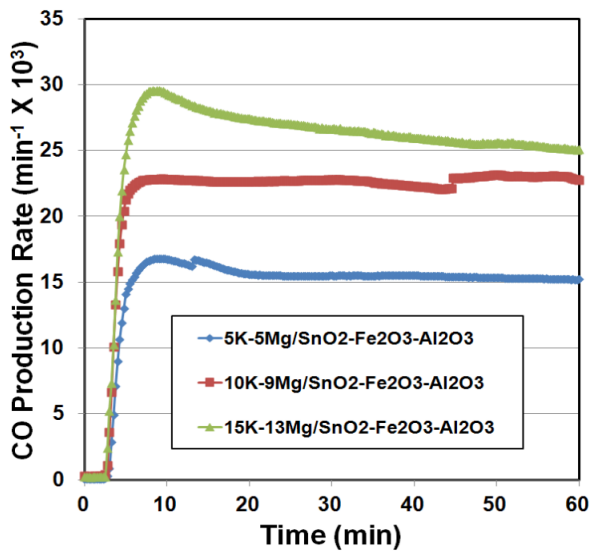

Figure 15. The CO_2 petcoke char gasification reactivity collected over the catalysts with various K and Mg loadings at 800 °C, 1 atm, and WHSV=2.36 h^{-1}

Parametric testing of catalyst composition continued with the goals of optimizing performance, evaluating the impact of composition changes on performance, and investigating the reaction mechanism. One of the compositional changes investigated was the concentration of Al_2O_3. Based on available information, the Al_2O_3 serves as a support material for the active components. One of the key functions for a support material is to provide surface area on which the active components can be dispersed. Catalysts with three different concentrations of Al_2O_3 were prepared at two different concentrations of alkali and alkaline earth metal concentrations. The BET surface areas determined for these samples are shown in Table 5. As expected, the catalyst surface area increased with Al_2O_3 concentration. However, Table 5 also demonstrates that increasing the alkali and alkaline earth metals resulted in a reduction of surface area. Figures 15 and 16 show the CO production rates for these catalysts.

Table 5. The surface area collected over the catalysts with various compositions

Catalyst	BET Surface Area (m^2/g)
10K-9Mg/SnO_2-Fe_2O_3-40Al_2O_3	29.7
15K-13Mg/SnO_2-Fe_2O_3-40Al_2O_3	19.9
10K-9Mg/SnO_2-Fe_2O_3-60Al_2O_3	60.8
15K-13Mg/SnO_2-Fe_2O_3-60Al_2O_3	44.7
10K-9Mg/SnO_2-Fe_2O_3-80Al_2O_3	77.6
15K-13Mg/SnO_2-Fe_2O_3-80Al_2O_3	56.2

Although the increase in the relative amount of support material was anticipated to improve performance by providing additional surface area for improved dispersion of the active components and promoters, the best performing catalysts in Figures 16 and 17 contained 60 wt% Al_2O_3 regardless of available surface area. Furthermore, the catalyst with the optimum performance was based on a maximum concentration of alkali and alkaline earth metal promoters and an Al_2O_3 concentration of 60 wt%. Analysis of performance and surface area revealed that surface area did not significantly affect the performance.

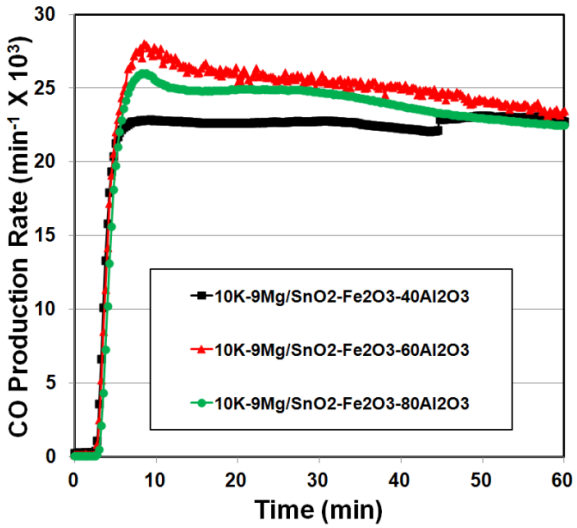

Figure 16. CO_2 petcoke char gasification reactivity collected over the catalysts with various Al_2O_3 contents and fixed loading of K and Mg at reaction conditions of 800 ˚C, 1 atm, and WHSV=2.36 h^{-1}

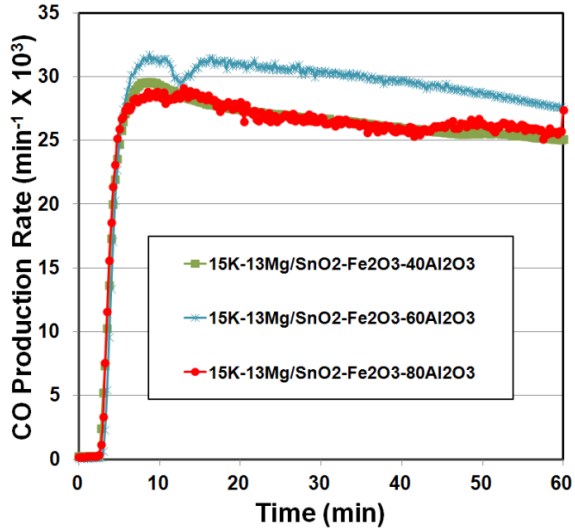

Figure 17. CO_2 petcoke char gasification reactivity collected over the catalysts with various Al_2O_3 contents and fixed loading of K and Mg at reaction conditions of 800 ˚C, 1 atm, and WHSV=2.36 h^{-1}

In previous testing, the effect of simultaneously increasing the K and Mg concentration in the catalyst while maintaining essentially the same ratio of K to Mg was investigated. In this next set of testing, the relative ratio of K to Mg was varied from 0.5 to as high as 2. The CO production rates for these catalyst formulations with petcoke char as a reductant are shown in Figure 18. The results in Figure 18 show that increasing the K to Mg concentration resulted in a higher and more stable CO production rate. However, the catalyst with higher K to Mg concentration also had the most rapid deactivation towards the end of the test. By contrast, the sample with higher Mg to K concentration had the lowest CO production. The higher Mg to K concentration also seemed to delay the initial onset of the decrease in the CO production rate and reduced the rate of decrease on the CO production rate throughout the test.

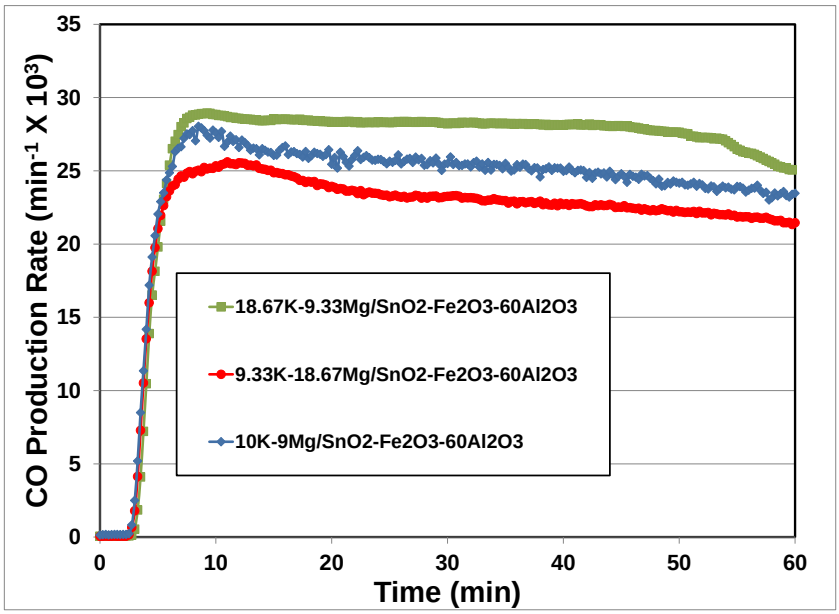

Figure 18. CO_2 petcoke char gasification reactivity collected over the catalysts with various Al_2O_3 contents and 10 K loading at reaction conditions of 800 °C, 1 atm, and WHSV=2.36 h^{-1}

4.6 Preparation of Spray-Dried Catalyst Formulations

For the preparation of the previous catalyst formulations, the main preparation procedure for the catalyst samples was based on an impregnation procedure. This effort focuses on the development of a new procedure that produces a spray-dried catalyst, which will be suitable as a fluidized-bed catalyst for operation of our transport reactor system for conversion of the carbon and CO_2 into CO. The two key characteristics that will be required for this fluidized bed catalyst are sufficient attrition resistance to ensure catalyst replacement costs can be minimized and high activity to maximize reaction rates during the short residence time in the reactor.

Our initial attempts at producing a fluid-bed catalyst by spray drying were with our K-Mg/SnO_2-Fe_2O_3-Al_2O_3 catalyst. This spray-dried catalyst formulation produced nearly spherical particles with a mean diameter of about 40 µm (which is standard for our spray drier). The Davison Index (DI), which is the standard measurement method for the attrition resistance for fluidized catalytic cracking (FCC) catalysts, was 2.7. The typical DI value for FCC catalysts measured in our system averages around 10.

The performance of this spray-dried catalyst was measured in our standard catalyst testing system. The results of this spray-dried catalyst and our best performing impregnated catalyst are provided in Figure 19. Figure 19 shows that the spray-dried catalyst has a slightly lower CO production rate, but demonstrates a similar stability of CO production for the entire 60 minute test. To explore the stability of this spray-dried catalyst past the typical 60 minute test period, special provisions were made to continue testing of this catalyst. Because our testing system does not have a means to continuously feed carbon into the reactor, the reactor was periodically reloaded with carbon by stopping the test and mixing the catalyst sample being tested with a fresh batch of carbon. Petcoke was selected as the preferred carbon source, because its low ash content would minimize ash accumulation and impact on the reaction. The results from this

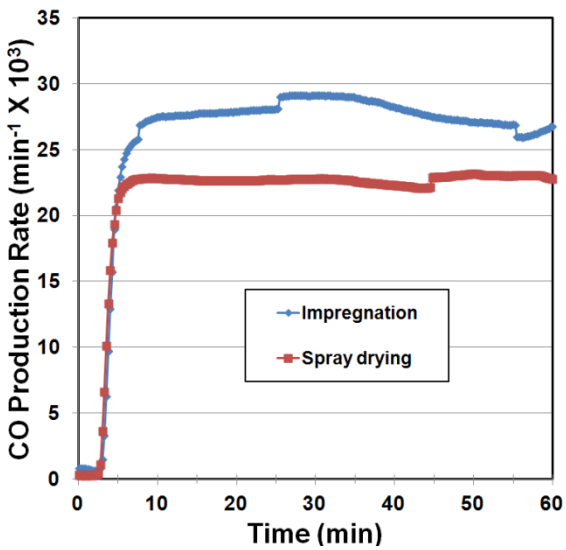

Figure 19. The catalytic CO_2 petcoke char gasification performances collected over the K-Mg/SnO_2-Fe_2O_3-Al_2O_3 catalysts prepared using different methods at 800ºC, and WHSV=2.36 h^{-1}

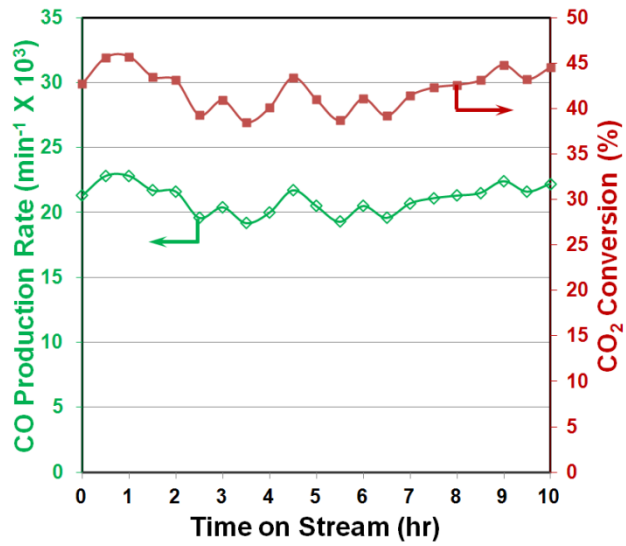

Figure 20. The catalytic petcoke char reactivity collected over the K-Mg/SnO_2-Fe_2O_3-Al_2O_3 catalyst prepared using spray drying method at 800 ºC, 1 atm, and WHSV = 2.36 h^{-1}

specialized test are shown in Figure 20. Although there is some variation in the CO production and CO_2 conversion over the 10 cumulative hours of testing potentially caused by the testing approach employed, these results strongly suggest stable catalytic activity for the spray-dried catalyst.

4.7 Parametric Reaction Testing

A variety of parametric testing was conducted to facilitate developing models to assist in simulating the process with Aspen and defining the catalytic reaction mechanism. The results from these tests are described in the following subsections.

4.7.1 Effect of CO_2 Concentration

Parametric testing of CO_2 concentration was conducted with CO_2/N_2 mixtures using switchgrass char as carbon feedstock at 800 ºC and gas hourly space velocity (GHSV) of 1,000 h^{-1}. The results shown in Figure 21 indicate that the CO production rate decreases consistently as the CO_2 concentration in the feed gas is decreased.

4.7.2 Effect of Weight Hourly Space Velocity (WHSV)

A second set of parametric tests were conducted at different weight hourly space velocities (WHSVs). The objective was to understand the relationship between gas/solid contact time and/or carbon concentration on reaction rate. The result in Figure 22 show that as WHSV decreases the net CO_2 conversion increases. This trend seems reasonable based on the fact that at lower WHSVs the net result is that the gas can be assumed to have longer contact with the carbon or that a higher amount of carbon is available for each gas molecule.

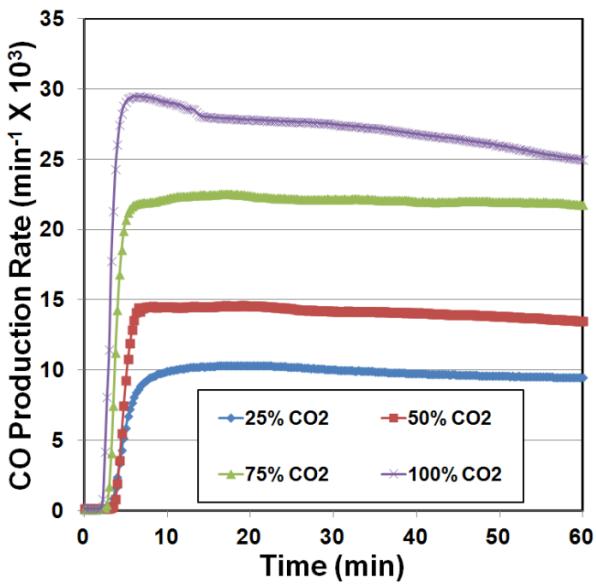

Figure 21. Switchgrass char reactivity during CO_2 gasification collected at 800ºC, 1 atm, GHSV=1,000 h^{-1}, and various CO_2 concentrations

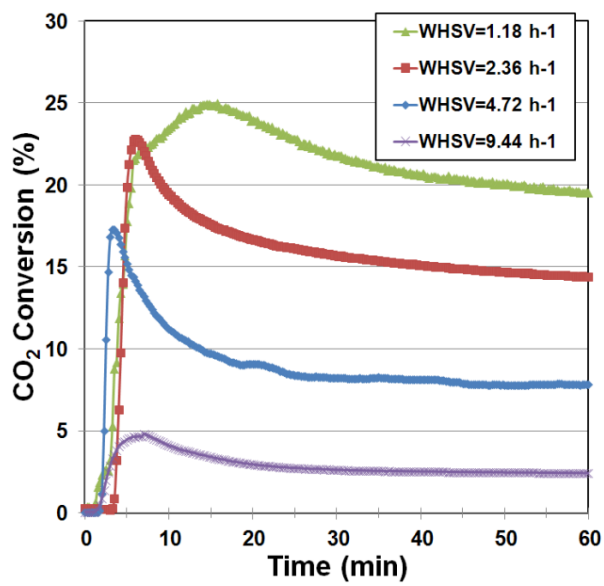

Figure 22. Switchgrass char reactivity during CO_2 gasification collected at 700 ºC, 1 atm, and various WHSV

4.7.3 Effect of CO on Reaction Rate

Multiple publications have demonstrated the presence of CO has an inhibiting effect on the reaction rate for the reaction between CO_2 and carbon Kajtani et. al. (2006) and Roberts et. Al. (2012). To evaluate the effect of CO on reaction rate, a test was conducted in which a 50/50 mixture of CO_2 and CO was used as the feed gas. The results in Figure 23 show that after the CO production rate has stabilized that the CO production is lower when a CO_2/CO mixture versus a CO_2/N_2 mixture is fed to the reactor. However, the reduction in CO production rate with the CO_2/CO mixture is much less than the decrease in CO production observed as the CO_2 concentration is decreased.

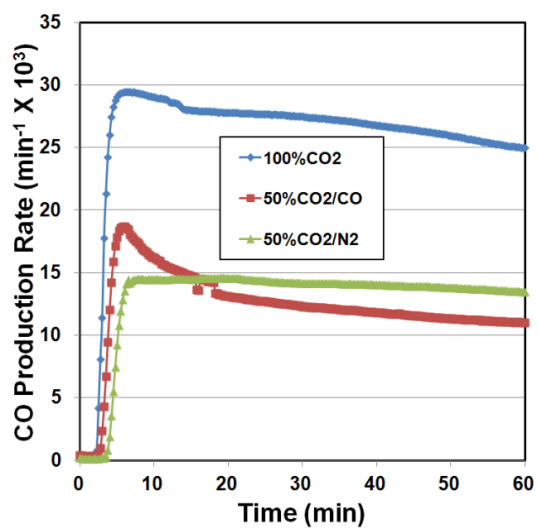

Figure 23. Switchgrass char reactivity under various feed compositions at 800ºC, and GHSV=1,000 h^{-1}

4.7.4 Effect of Catalyst Pre-reduction on CO Production

Effective catalysts for the reaction between carbon and CO_2 must be able to effectively transfer oxygen from CO_2 to carbon. Because of the high stability of the CO_2 molecule, the only means to effectively remove oxygen from CO_2 is to extract the oxygen by means of a reduction reaction. As the reaction takes place under reducing conditions, the natural state for the catalyst would be reduced. Therefore to demonstrate the ability of the reduced catalyst to extract an oxygen from

CO_2, the catalyst was pre-reduced with a 5% H_2 in N_2 mixture prior to exposure to a CO_2 feed stream. The results from this test are shown in Figure 24. These results do confirm that the two most promising catalyst formulations, when reduced, are very effective for converting CO_2 into CO by extracting an oxygen.

As part of this testing, the reaction between the unreduced catalyst and CO_2 was also tested at same operating conditions. These results are also shown in Figure 24 and are very interesting because the unreduced catalysts also resulted in an appreciable amount of CO production. This is very interesting because even in what would be expected to be an oxidized state, these catalysts demonstrated the ability to reduce CO_2 by extracting an oxygen. If these catalysts also have the ability to effectively release the oxygen to carbon at different levels of oxidation, these catalysts will be able to catalyze the extraction of oxygen from CO_2 and the reaction between this extracted oxygen and carbon.

Another interesting feature about the results from the unreduced catalyst test is the CO concentration profiles. Each catalyst has its own unique CO concentration profile. For the K-Mg/SnO_2-Fe_2O_3-Al_2O_3, the CO concentration profile rapidly increases, but remains relatively constant for the remainder of the test. By contrast, the CO concentration profile for the K-Ca/ZnO-CeO_2 catalyst suddenly after about 7 minutes of exposure to the CO_2 reactant increases to a maximum and gradually decreases for the remainder of the test. One potential explanation of these different CO concentration profiles is a different rate limiting step in the reaction mechanism for these two catalysts.

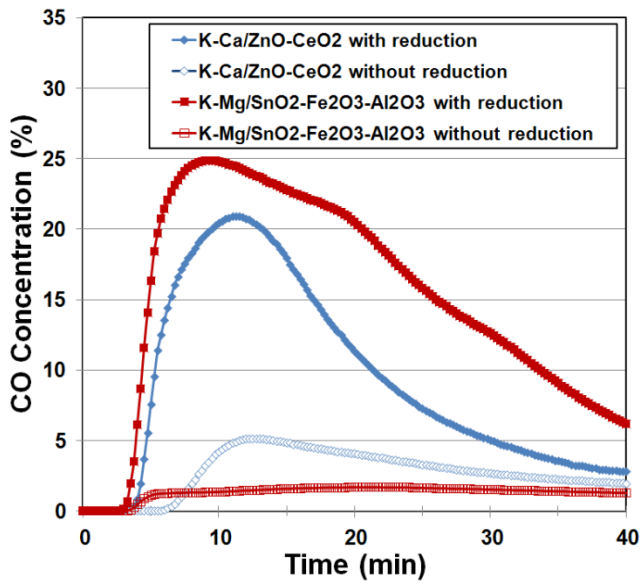

Figure 24. The CO production profiles collected at 800 °C and 1 atm for CO_2 reduction capability evaluation of two catalysts with and without H_2 pre-reduction

Consider breaking down the reaction into three fundamental steps: (1) adsorption of CO_2, (2) reaction of the CO_2 with the catalyst, and (3) desorption of the CO product. If the desorption step is the rate limiting step, the CO_2 would rapidly adsorb onto the catalyst and react. However, release of the CO product would be controlled by the rate limiting desorption step and result in a steady and constant CO concentration like for the K-Mg/SnO_2-Fe_2O_3-Al_2O_3 catalyst. If the rate of desorption was slow enough, the CO concentration profile would reflect this steady but slow desorption rate even though the number of reduced sites for this reaction were being consumed by the reaction.

If alternatively, the CO_2 adsorption was the rate limiting step, the concentration of adsorbed CO_2 species would gradually grow on the catalyst. However once adsorbed, the CO_2 would rapidly react and release the CO product. If the adsorption rate is faster that the rate at which available reduced site on the catalyst are consumed, the CO concentration profile would go through a

maximum and subsequently decrease at a rate that was related to the consumption of the reduced catalyst sites.

4.7.5 Use of Controlled Carbon Species to Investigate Catalytic Reaction Mechanism

Although the ultimate goal for catalyst development is to be able to catalyze the CO_2 carbon reaction for abundant low cost carbon sources like coal, petcoke, and biomass, these carbon sources are very complex and do not readily permit investigation of the catalytic reaction mechanism. To overcome this limitation, the catalytic reaction with specific hydrocarbon species can be tested to facilitate developing a model for the catalytic reaction mechanism. During this quarter, the catalyst was tested with a methane/CO_2 mixture. The results from this test are shown in Figure 25. Figure 25 shows that the catalyst does catalyze the reaction between CO_2 and CH_4. When the production of CO and H_2 has stabilized, roughly equal amounts of CO and H_2 are produced as would be expected if CH_4 was reacting with the CO_2.

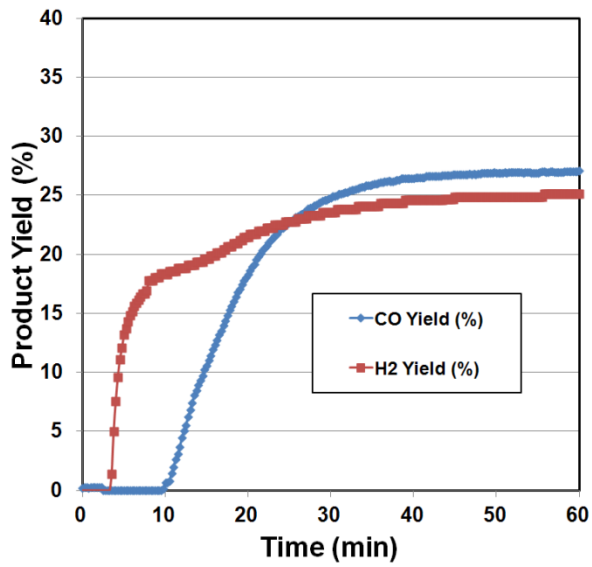

Figure 25. The methane dry reforming activity of the K-Mg/SnO_2-Fe_2O_3-Al_2O_3 catalyst collected at 800 ^oC and WHSV=2.36 h^{-1}

The odd feature about Figure 25 is that the production of CO and H_2 do not follow the same pattern. The H_2 rapidly increases to a yield of about 15% and then more gradually increases to about 25%. The CO yield remains near zero for about 10 minutes and then steadily increases to a yield of about 27%. In the previous section, testing with CO_2 suggested that desorption of the CO product was the limiting step in the reaction sequence with CO_2 for this catalyst (K-Mg/SnO_2-Fe_2O_3-Al_2O_3). In this test, the first product formed is H_2, which could only come from reaction of the catalyst with CH_4. This would suggest that adsorption of CH_4 and dehydrogenation of the CH_4 is more rapid than CO_2 adsorption. As the primary active phase on the catalyst is present in its oxidized state at the start of the test, this would promote more rapid adsorption of the CH_4 than CO_2. However, after all the oxidation sites are consumed, the number of reduced sites would have increased and the rate of CO_2 adsorption and reaction would increase. This is observed to occur at roughly 10 minutes into the test. As the CO_2 is adsorbed and reacted, it reoxidizes catalytic sites for adsorption and dehydrogenation of the CH_4 enabling hydrogen production to increase. The rate of H_2 production increases more slowly than CO production because desorption of CO from the catalyst is slower so the rate at which catalytic sites are freed up for reaction with methane is slower.

4.7.2 Effect of Catalyst /Carbon Contact

A fundamental requirement for a catalyst to impact reactivity is physical interaction between the catalyst and reactants. This is typically accomplished by actual physical contact between the catalyst and reactant. For mobile gas phase reactants, the reactants can readily move to achieve

physical contact with the catalyst. However, for CO_2 gasification reactions necessary for CO_2 utilization in this project, the ability to achieve intimate physical contact between the CO_2, carbon, and catalyst presents a challenge as neither the solid carbon nor solid catalyst is capable of moving to achieve intimate contact in a fixed bed. In previous attempts to catalyze reactions with coal, one promising solution was to effectively use the coal as a support and impregnate or deposit the catalyst onto the coal. However, a significant disadvantage of this approach was that separation of the catalyst from resulting char/ash made recover of the catalyst for reuse cost prohibitive.

In spite of this disadvantage, we wanted to investigate the impact on reactivity resulting from enhanced the physical contact between the catalyst and reactant. We focused on impregnation, because of the success with previous impregnation approaches. One of the first problems, we encountered was our most reactive catalysts were based on combinations of multiple compounds. Furthermore, the solubility of the standard precursors we employed was not suitable to impregnate the most active composition. To overcome this issue, we attempted to use nitrate precursors, well known for their high solubility.

Our next challenge was to calcine the catalyst precursors effectively changing them into the active catalytic components. Calcination of these catalyst impregnated carbon sources could not be conducted in air, because the air would oxidize the carbon at the high calcinations temperature. To avoid carbon oxidation during calcination, nitrogen was used as a purge gas during calcinations and the calcinations temperature was reduced to the bare minimum necessary for decomposition of the catalyst precursors. Even with these precautions, excessive loss of carbon occurred during calcination. As a consequence of these issues, all attempts to impregnate the carbon sample with catalyst were abandoned.

5. Reaction Mechanism Investigation

5.1 Thermogravimetric Testing

During thermo-gravimetric (TGA) testing, a sample of the most promising catalyst sample was exposed to sequential purge, reduction, and oxidation periods to identify patterns in the weight loss profiles for the catalyst. To start these tests, the catalyst was initially heated in a nitrogen atmosphere to remove any residual chemical species on the catalyst. After removing these residual gas species, the catalyst was exposed to a 10% CO in N_2 gas mixture as the temperature was ramped from 30ºC to 800ºC. After cooling and purging the reducing gas from the system, the catalyst was exposed to CO_2 while heating from 30ºC to 800 ºC. Figure 26 shows, during this test, the catalyst experienced a weight gain during exposure to CO_2 that was essentially identical to the weight loss during reduction. During three repetitive reduction and oxidation exposures, the catalyst consistently demonstrated that the weight gain during exposure to CO_2 was essentially identical to the weight loss during reduction.

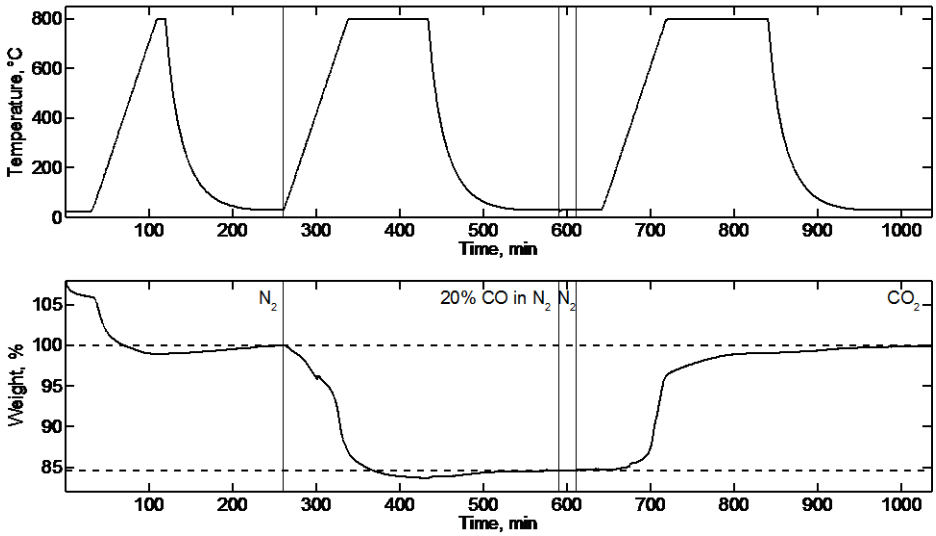

Figure 26. Weight loss profiles during TGA reduction with CO in N_2 and oxidation with CO_2

In the next test, the catalyst was exposed to CO_2 and then air to identify any differences in oxidation that result when these different oxidants are used. After an initial reduction in a 10% CO in N_2 mixture, the catalyst was exposed to CO_2 and heated from 30ºC to 800ºC. After cooling the catalyst back to 30ºC and purging with N_2, the catalyst was exposed to air and heated from 30ºC to 800ºC. Figure 27 shows that during this subsequent oxidation with air, the catalyst gained only a minimal amount of weight. This demonstrates that the reduced catalyst was completely oxidized with CO_2.

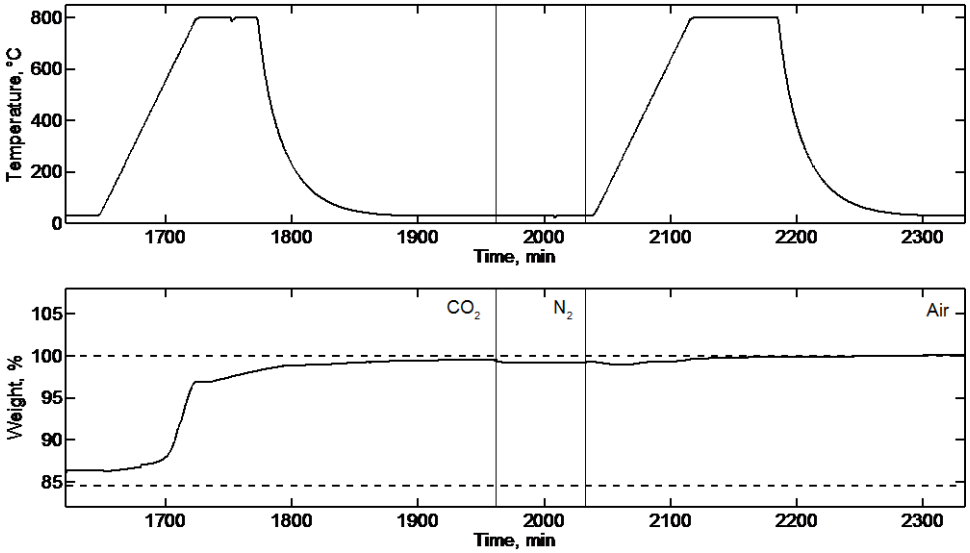

Figure 27. Weight loss profiles during TGA oxidation with CO_2 and air

In the next experiment, the reduced catalyst was cooled and heated in nitrogen, prior to heating from 30ºC to 800ºC in air. The results, shown in Figure 28, confirm that the weight gain during oxidation with air is identical to the weight gain that occurs during oxidation with CO_2.

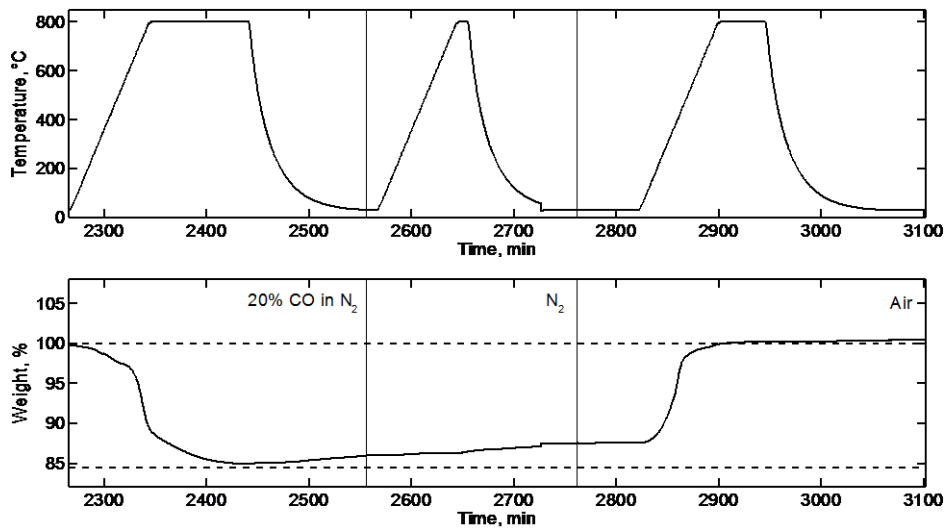

Figure 28. Weight loss profiles during TGA reduction and oxidation with air

5.2 Autochem Testing

The fact that the reactor effluent in the Autochem system is monitored with a mass spectrometer (MS) provides a unique means of monitoring the chemical species present in the reactor effluent. In the particular reduction and oxidation sequence of interest for our catalyst, it also enables the use of labeled CO_2 with ^{18}O (a naturally occurring isotope of oxygen with an atomic mass of 18 instead of 16) to track the transfer of oxygen from reactant to catalyst and ultimately to gas phase product.

The testing sequence in the Autochem was similar to the tests conducted in the TGA. The catalyst was initially heated in He (He was used instead of N_2 because N_2 would interfere with MS response for CO) from 30ºC to 800ºC to remove any residual gas species on the catalyst. After removal of these residual gases, the catalyst was reduced in a 20% CO in He. Figure 29 provides the MS profiles for this reduction and shows the reduction that occurs at approximately 800ºC results in a decrease in CO concentration in the product that is mirrored by an increase in CO_2 concentration. These results confirm that the CO is reducing the catalyst by removing oxygen from the catalyst converting the CO reactant into CO_2.

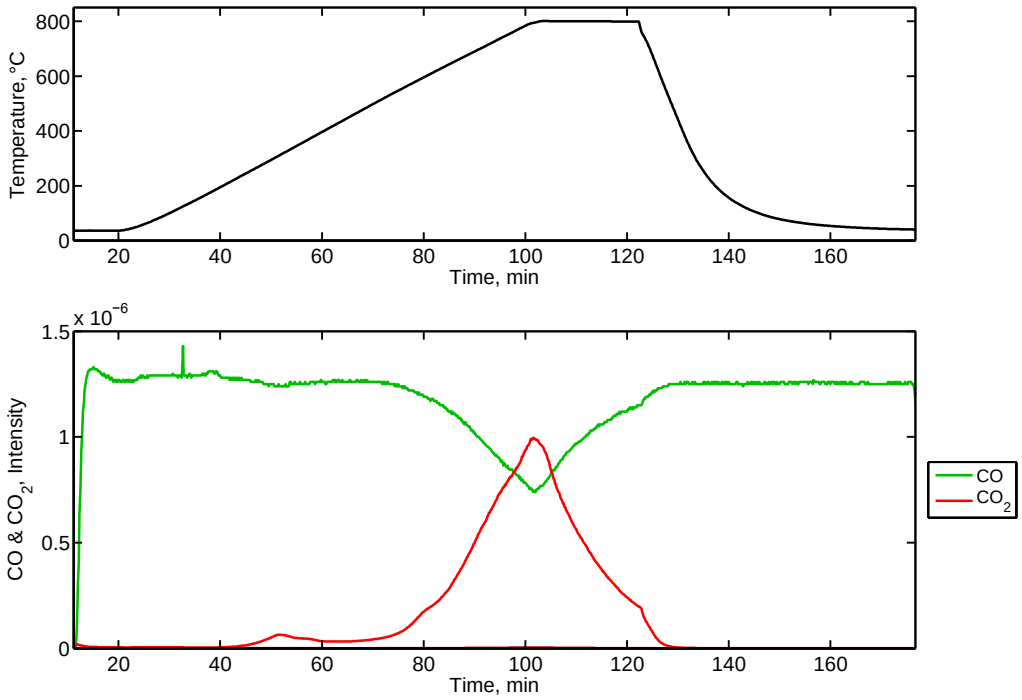

Figure 29. MS profiles during exposure of the catalyst to 20% CO in He while heating from 30ºC to 800ºC

In the next step, the reduced catalyst was exposed to $C^{18}O_2$. The objective was to investigate if the labeled oxygen is transferred to the catalyst during oxidation. Figure 29 shows the MS profiles for the reactor effluent during the heating from 30 ºC to 800ºC in $C^{18}O_2$. Figure 30 shows a dip in the effluent concentration of $C^{18}O_2$ and spike in the effluent CO and $C^{18}O$ concentrations at approximately 800ºC. The dip in $C^{18}O_2$ and the spike in $C^{18}O$ confirm the transfer of labeled oxygen to the catalyst. The spike in CO suggests that available oxygen on the catalyst surface can also be exchanged with the oxygen in the $C^{18}O_2$ molecule when it is adsorbed onto the catalyst surface. These results indicate that the reaction mechanism does result in removal of oxygen from CO_2 onto the catalyst and that the oxygen on the catalyst surface is relatively mobile.

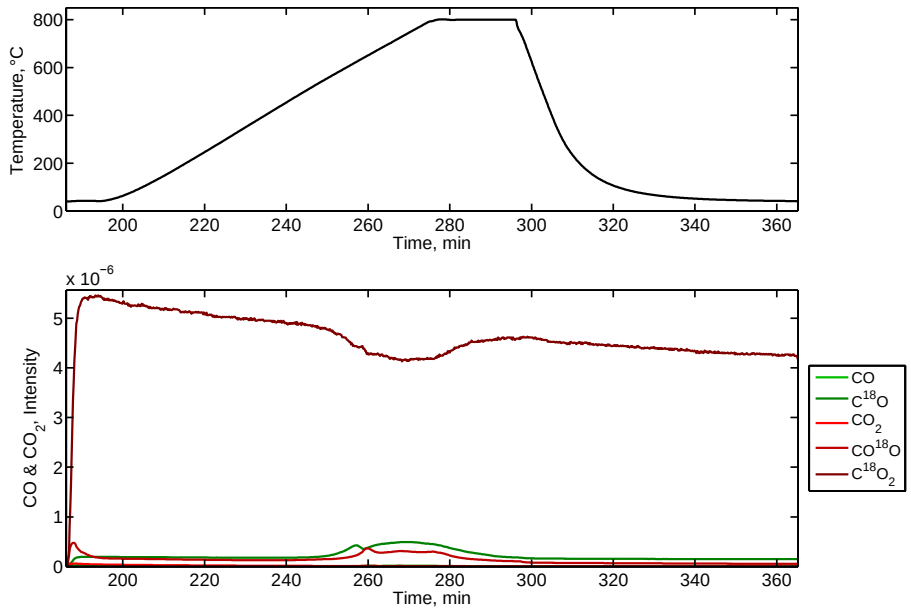

Figure 30. MS profiles during exposure of the catalyst to $C^{18}O_2$ while heating from 30ºC to 800ºC

In the final segment of this test, the catalyst was re-exposed to 20% CO in He and heated from 30ºC to 800ºC. The primary goal of this exposure was to demonstrate that the labeled oxygen placed on the catalyst during exposure to $C^{18}O_2$ could also be successfully removed from the catalyst by reduction with CO. Figure 31 shows that at about 800ºC, the concentration of CO in the effluent gas drops. As the CO concentration in the effluent drops, the concentrations of $C^{18}OO$, $C^{18}O_2$, and CO_2 also increase. This clearly demonstrates that the labeled oxygen can be removed during reduction. The fact that all three potential oxygen combinations are observed also confirms the theory that oxygen on the catalyst is extremely mobile. The observation of a $C^{18}O$ peak helps demonstrate that the oxygen mobility/transfer on the surface is faster than the adsorption/desorption processes for both CO and CO_2. The net results from these three tests show that this catalyst can effectively remove oxygen from CO_2 and subsequently use this oxygen to oxidize CO.

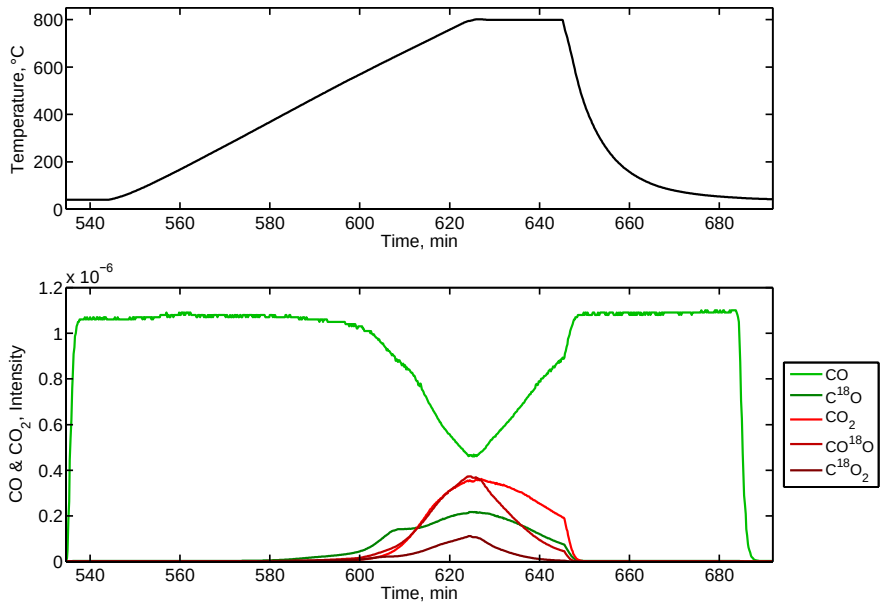

Figure 31. MS profiles during exposure of the catalyst to 20% CO in He while heating from 30ºC to 800ºC after exposure to $C^{18}O_2$

5.3 Bench-scale Testing

The primary objective of the bench-scale testing was to demonstrate that carbon could be used as a reductant for the catalyst producing CO as a product. A series of preparation steps were performed to subject the catalyst to the same preparatory steps used in the Autochem and TGA tests. These steps included the initial heating and inert purging to remove any residual gas on the catalyst, initial reduction of the catalyst with 10% CO in nitrogen, and oxidation of the catalyst with CO_2. In each of these steps, analysis of the effluent gas confirmed increases or decreases in the CO and CO_2 concentration similar to those observed in the Autochem and TGA testing. After preparation of the catalyst had been completed, an approximately equal mass of petcoke char was added to the catalyst bed in the reactor while maintaining a N_2 purge to avoid any air exposure of the catalyst.

The catalyst and petcoke sample was heated in N_2 from 30ºC to 800ºC. Figure 32 shows the CO and CO_2 effluent concentration profiles during this test. The key feature of the effluent concentration profiles in Figure 32 is the peak in both CO_2 and CO concentration that occurs at approximately 800ºC. This peak occurs in the same temperature range in which peak catalyst activity for oxygen donation from the catalyst was observed in the TGA and Autochem testing. The production of both CO_2 and CO shows that the catalyst can effectively provide sufficient oxygen to result in complete oxidation of any available carbon. This test is different from previous tests conducted in the bench-scale system in that no CO_2 was added to the reactor while the sample was heated from 30ºC to 800ºC. Without the CO_2 in the gas feed to suppress complete oxidation, the oxygen available on the catalyst would preferentially completely oxidize the carbon and produce CO_2. Thus, the higher production of CO_2 over CO is the expected result for this test.

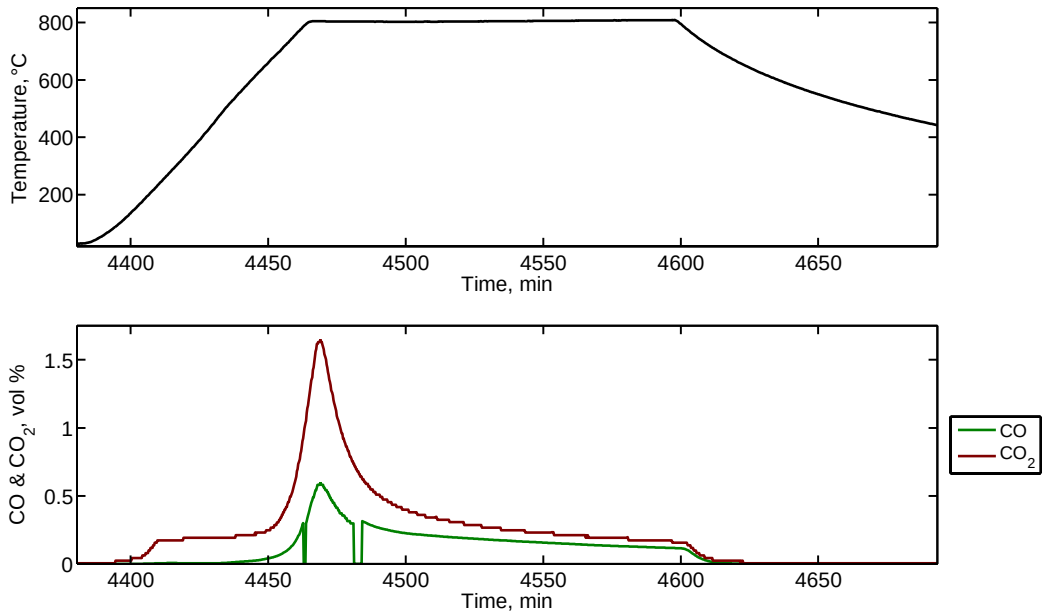

Figure 32. Reactor effluent profiles for catalyst and petcoke during heating from 30ºC to 800ºC and after exposure to reduction and exposure to CO_2

Other minor features of the profile in Figure 32 have not been seen in the previous results obtained from the Autochem and TGA systems. These minor features include the fairly constant CO_2 production that begins at 200ºC and continues to 700ºC and the lingering concentrations of CO_2 and CO in the effluent gas while the catalyst and petcoke mixture are maintained at 800ºC. Neither of these features was observed in the Autochem or TGA Tests. Consequently, the most probable explanation is that these products are associated with the primary difference between those tests and this test, which is the presence of petcoke char.

Petcoke is a waste product composed of the least reactive carbon species in a petroleum refining process. Although the raw petcoke product was preheated in a preparatory process to convert it to char, it still retains some more reactive hydrocarbon species. It is extremely likely, that the CO_2 production between 200ºC and 700ºC was generated from reaction of these reactive hydrocarbon species and the catalyst. Similarly, the tail CO_2 and CO production at 800ºC probably represents the slow oxidation of the least reactive hydrocarbon species present in the petcoke char.

These results definitively confirm that the promising catalyst candidate being tested could effectively take oxygen from CO_2 and use this oxygen to oxidize the hydrocarbon species in petcoke.

6. Evaluation of Potential Chemical Intermediates

The ability to control the extraction of oxygen from CO_2 and effectively use this oxygen for controlled oxidation of hydrocarbons generates many opportunities for synthesis of a very large set of chemical intermediates. The key challenge was to focus our R&D efforts on the most promising opportunities based on likelihood of success with our current understanding of the

reaction mechanism and the potential impact on the chemical intermediate production. To meet this challenge, we chose to employ a ranking strategy that would identify the most promising chemical intermediates based on potential success of employing the reaction mechanism and benefits for the project.

In this ranking strategy, the team members were asked to rank each chemical intermediate based on a list of criteria for potential for success and benefits for project. The specific lists for chemical intermediates, likelihood of success, and project benefits are provided in Table 6, 7, and 8, respectively. The response for the team members were collected and collated. Figure 33 displays the results from this ranking process and effectively organizes the most promising intermediates in the upper right quadrant.

From Figure 33, the most promising chemical intermediates are syngas, methanol, and ethylene oxide. Syngas, which consists of a mixture of H_2, CO, CO_2, and steam, has been the product gas that we have used to evaluate carbon source activity and catalyst development/optimization. Because of the current state of development for this product, we have focused our efforts on completing a preliminary process economic analysis for syngas production. The details of this process economic analysis are provided in the following section. As the promising reaction mechanism we have discovered also has the promise to enable direct CO_2 conversion into higher value chemical products, we refocused our catalyst development efforts to evaluate and identify catalyst formulations for direct CO_2 conversion into marketable chemicals. The catalyst development efforts are described in the section following the process economic analysis.

Table 6. Chemical intermediates evaluated with ranking strategy

Hydrocarbon Family	Chemical Intermediates
H_2 and CO	Syngas
C_1	Methanol, formic acid, formaldehyde
C_2	Ethylene, ethylene oxide, ethanol, DME, acetic acid, acetaldehyde, methyl formate
C_3	Propylene, propylene oxide, acetone, propionic acid, acrylic acid
C_4	Butanol, methyl methacrylate
C_{4+}	Phenol

Table 7. Criteria used to quantify project benefits

Project Benefit	Key Questions	Weighting
Technology entry barriers	Can the technology overcome barriers for commercial application?	1
Scientific stature	Will the research provide opportunities for publications or conference presentations?	1
Market opportunity	What is current market size? How fast is the market expanding?	1
Value proposition	Does CO_2 utilization increase because of improved CAPEX, OPEX, etc?	1
Intellectual property	Can this technology provide a competitive edge?	1

Table 8. Criteria used to quantify likelihood of success

Project Benefit	Key Questions	Weighting
Operating Temperature	Can current reaction mechanism be successfully extended to lower operating conditions?	3
Reaction complexity	How much additional reaction complexity will be added to insert the oxygen into the hydrocarbon to make the chemical intermediate?	3
Catalyst modification	What level of catalyst modification and optimization will be necessary to make the chemical intermediate?	3
Testing capabilities	Are the necessary testing systems available and suited for the testing necessary to support this R&D effort?	3
Evaluation of reaction mechanism	What level of understanding of the reaction mechanism will be necessary to successfully make chemical intermediates?	3
Reactant phase	How does the reactant phase affect reactor design and complexity?	1
C to H ratio of reactant	Is the chemical composition of the reactant suitable to product the chemical intermediate?	1
Value addition	Does the new process provide significant value creation during production of the chemical intermediate?	1
Impurities	How will impurities affect the catalyst and/or production process?	1
Operating pressure	Will the reaction chemistry favor high pressure operating conditions?	1
Complexity of current process	Does the new process offer a reduction in processing complexity?	1

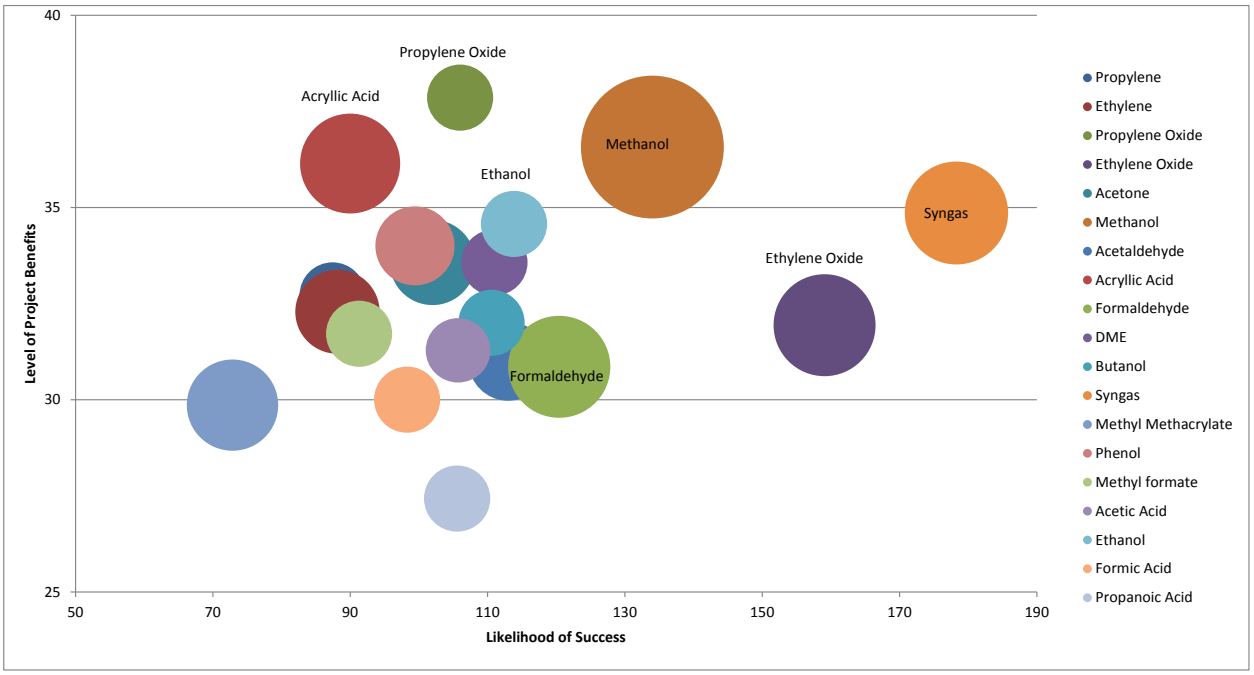

Figure 33. Results from ranking strategy used to assess most promising chemical intermediates

7. Process Economics of CO_2 Utilization for Syngas Production

A syngas product was chosen because it is an optimal starting mixture for subsequent synthesis of methanol, dimethylether (DME), gasoline, and Fisher Tropsch (FT) wax and diesel. The block flow diagram for the base case, shown in Figure 34, is based on the flue gas generated from a 75,000 bbl per day fluid catalytic cracking (FCC) system. The flow rate and composition for the flue gas was estimated based on circulation of 55,900 metric tons per day of FCC catalyst with 3 wt% coke.

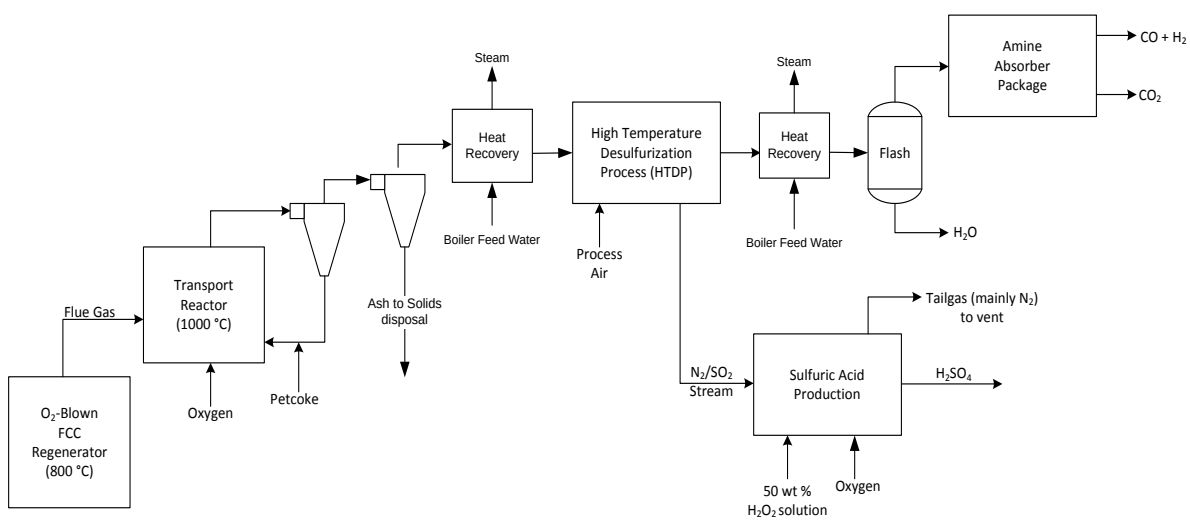

Figure 34. Block Flow Diagram of the CO_2 utilization process

This process economic analysis consisted of the following sequential steps:

- Develop a representative set of detailed process flow diagrams (PFDs) which effectively includes all the equipment directly necessary for the process and any additional equipment necessary to support the process (i.e., balance of plant systems),
- Develop heat and mass balances for the plant described by detailed PFDs,
- Use the detailed PFDs and heat and mass balances to develop a sized equipment list, which includes any special or required specifications,
- Obtain cost estimates for all the equipment,
- Apply standard factored estimates to generate a total installed capital cost, and
- Develop a detailed cash flow model for the life expectancy of the plant.

During development of the detailed PFDs, all heat recovery and integration options investigated during development of the general block flow diagram were incorporated. However, two key simplifications were implemented with the knowledge that additional details could be included in subsequent revisions of this process economic analysis. The first simplification was to assume that the carbon feedstock is delivered suitably processed for direct feed into the process. To compensate for the processing costs, a reasonable premium was included in the effective cost for the feedstock. Although this simplification overlooks the complexity of the processing systems necessary for preparing some of the feedstocks being considered, it enabled differing selection of a specific carbon source until more experimental information about carbon source reactivity was available. As this information becomes available, more details concerning feedstock preparation can be included in the base case economic analysis.

The second simplification was to accept a low pressure mixture of H_2 and CO as a marketable syngas product. This simplification was strategically selected to generate a base case system that could be used in the future economic analyses for production of more commercially attractive chemicals including methanol, dimethyl ether, gasoline, diesel and other Fischer-Tropsh liquids.

Aspen Plus was used to model the process and generated mass and energy balances. An Aspen Plus model for the CO_2 utilization process based on a transport reactor system was developed using a modified equilibrium-based reactor. The predicted outcome from this Aspen Plus model was confirmed based on results generated during CO_2 gasification testing with petcoke in the fluidized-bed reactor system. The Aspen Icarus Process Evaluator (IPE) was used to generate equipment costs from the sized equipment list. Factored costs were included for engineering, permits, licenses, and contingency.

During development of the cash flow model, many of the assumptions made were selected to reflect typical commercial and financial realities faced by any new commercial plant. A summary of these assumptions is provided in Table 9. Throughout this effort, we attempted to include the level of detailed that would be used for justifying the financial decision for installing a new commercial plant.

Table 9. Assumptions made during development of cash flow model

Assumption	Details
Plant life	20 years
Plant availability	Initial plant availability 80% increasing 5% per year and remaining at 95% availability after four years of operation
Financing	60% leveraged based on capital cost
Escalation	Raw material and product prices were assumed to escalate over plant life
Operational costs	Debt payment, maintenance costs, personnel wages, insurance, and property tax were included in cash flow analysis

Based on the analysis completed, the total installed capital cost was $778 million with a project internal rate of revenue (IRR) of 46%. We think that this unusually high IRR reflects two facts. The first is that our simplifying assumptions for processing the carbon feedstock and syngas product may have been too simplistic to adequately capture the costs associated with these processes. Even if implementing improvements to more appropriately address our simplifying assumptions were to reduce the IRR by half, the resulting IRR would still be very promising. This highlights the second fact, which is that the process seems to have a significant potential to be financially viable.

To help focus the experimental efforts for process development on issues that would have the most significant impact, we also performed sensitivity analysis to identify the most critical factors influencing the process profitability. The results for this sensitivity analysis are presented in Figure 35. The most important factor affecting process profitability was the product price. Although the actual analysis altered product price, the product price is used to estimate the net yearly revenue generated. The key process variable that would affect this value would be conversion. The sensitivity analysis also indicated that capital cost and oxygen price had a modest effect on IRR. The production of additional electricity and cost of the petcoke had only a small effect on IRR.

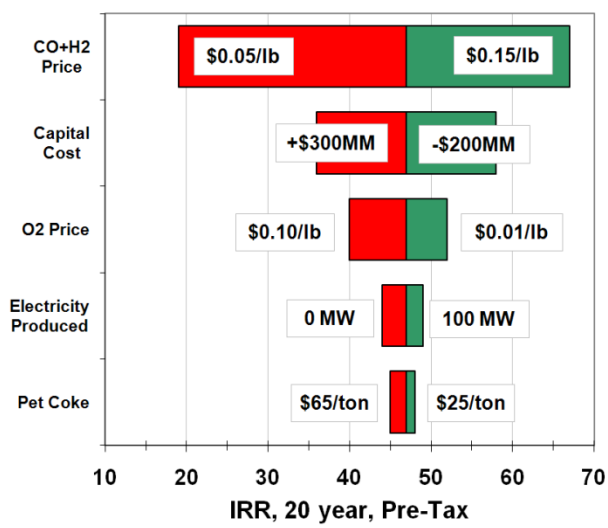

Figure 35. Sensitivity analyses of CO_2 utilization process

8. Catalyst Development for Direct Chemical Conversion

During evaluating the criteria for the likelihood of success for our raking exercise of the chemical intermediates, the three key challenges that our project team identified were:

- Catalytic oxygen extraction activity occurred at temperatures typically higher than used for synthesizing most chemical intermediates,
- Conversion of the raw hydrocarbon into the desired chemical intermediate required both a very selective and targeted oxidation reaction for yields that would be commercially attractive, and
- Selection of the appropriate hydrocarbon feedstock that could be effectively converted into a desirable product by the selective oxidation being catalyzed.

However if these three challenges could be overcome, almost all the chemical intermediates evaluated could be potential applications for this catalytic technology.

To exploit this opportunity, we chose to focus catalyst development efforts on the first two challenges. Our intention was to use combinations of mixed metal oxides to create catalysts with oxidation/reduction activity with CO_2 as the oxidant at temperatures below 500°C

In addition to investigating catalyst formulation for reducing the temperature of the reduction/oxidation activity of the catalyst, we also investigated catalysts/promoters that could be incorporated in the catalyst to improve the reactivity and selectivity of the hydrocarbon oxidation. Because this is another catalytic function of mixed metal oxides, including this additional constraint helped refine our catalyst development efforts to approximately 4 mixed metal oxide families. The anticipated improvement and rationale for this improvement for the different catalyst families are shown in Table 10.

Table 10. Chemical intermediates evaluated with ranking strategy

Catalyst Family		Rationale
A	• Lower temperature for oxygen extraction from CO_2 • Lower reaction temperature for hydrocarbon oxidation	Literature data demonstrates oxidative methane coupling on other supports using air
B	• Lower reaction temperature for hydrocarbon oxidation	Literature data demonstrates low temperature oxidations of VOCs, water, and nitrogen oxides
C	• Lower reaction temperature for hydrocarbon oxidation	Commercially used for synthesis of methanol from syngas as well as carbon dioxide
D	• Lower temperature for oxygen extraction from CO_2 • Lower reaction temperature for hydrocarbon oxidation	Literature data demonstrates dry methane reforming on other supports and as co-catalysts with other metals than iron

As different formulations for the different catalyst families were completed, these catalysts were initially subjected to TPR in a gas mixture containing 5 vol% hydrogen. This testing was

conducted to investigate the potential of the new catalyst formulation to shift the reduction temperature of the iron oxide to lower temperatures. Three of the catalyst families identified did shift the temperature peaks for iron oxide reduction to lower temperatures. Figure 36 shows the reduction profile as a function of temperature for the original catalyst formulation and these three catalyst families. The vertical dotted line in all the profiles represents the temperature of the peak in the reduction profile for iron oxide for the original catalyst.

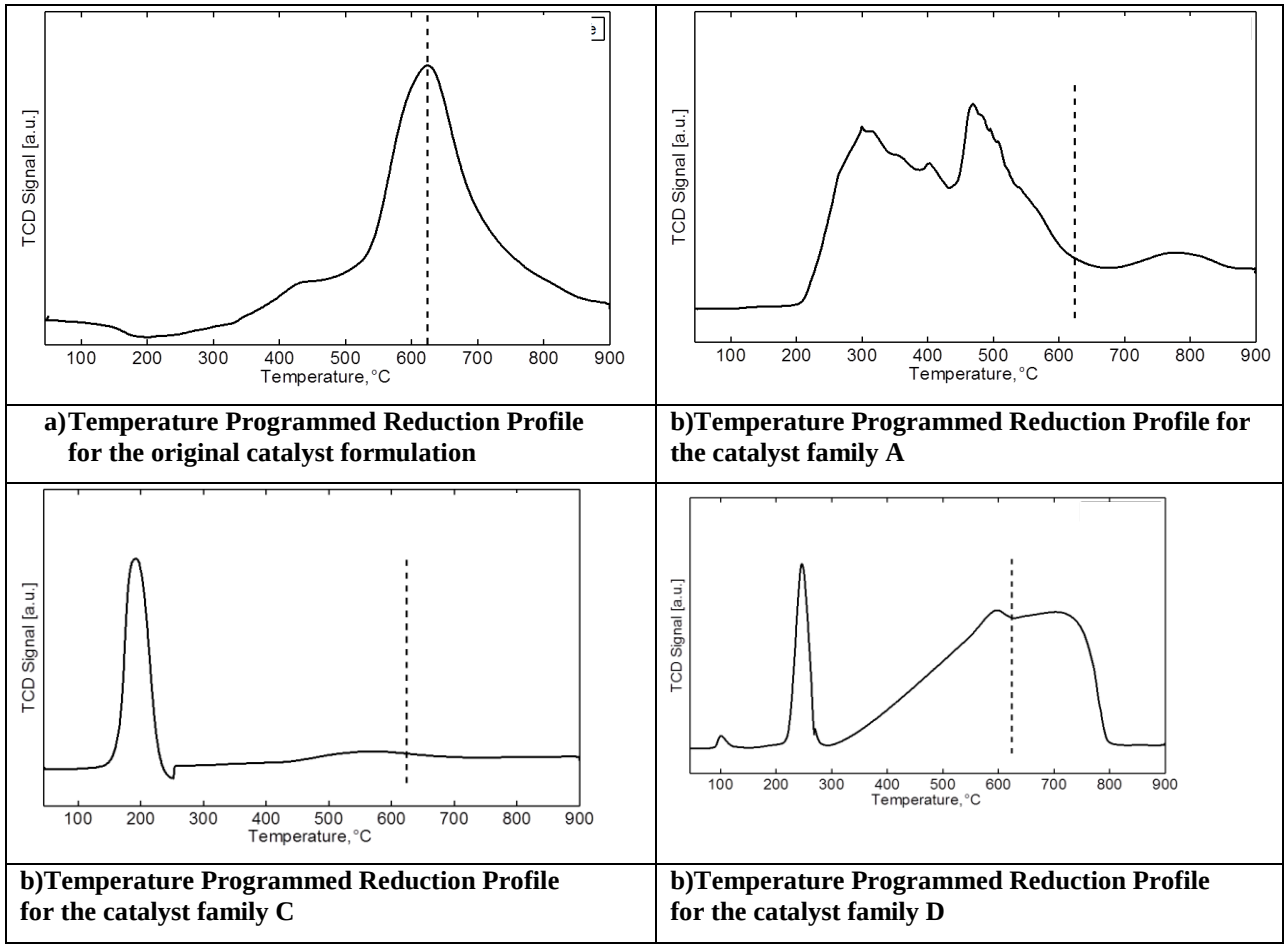

a) Temperature Programmed Reduction Profile for the original catalyst formulation

b) Temperature Programmed Reduction Profile for the catalyst family A

b) Temperature Programmed Reduction Profile for the catalyst family C

b) Temperature Programmed Reduction Profile for the catalyst family D

Figure 36. Results from TPR screening of catalyst formulations for the different catalyst families

8.1 Catalysts screening

After the initial TPR screening, the catalyst samples were tested in the TGA-MS system. The specific reaction sequence included a reduction with CO, an oxidation with CO_2 followed by a reduction with methane. No unusual observations were made during the CO reduction step. During the CO_2 oxidation step, three of the catalyst families demonstrated at least some weight increase resulting from oxidation of the catalyst at temperatures significantly below the 800°C observed for the original catalyst. The weight and temperature profiles for these three catalysts are shown in Figure 37.

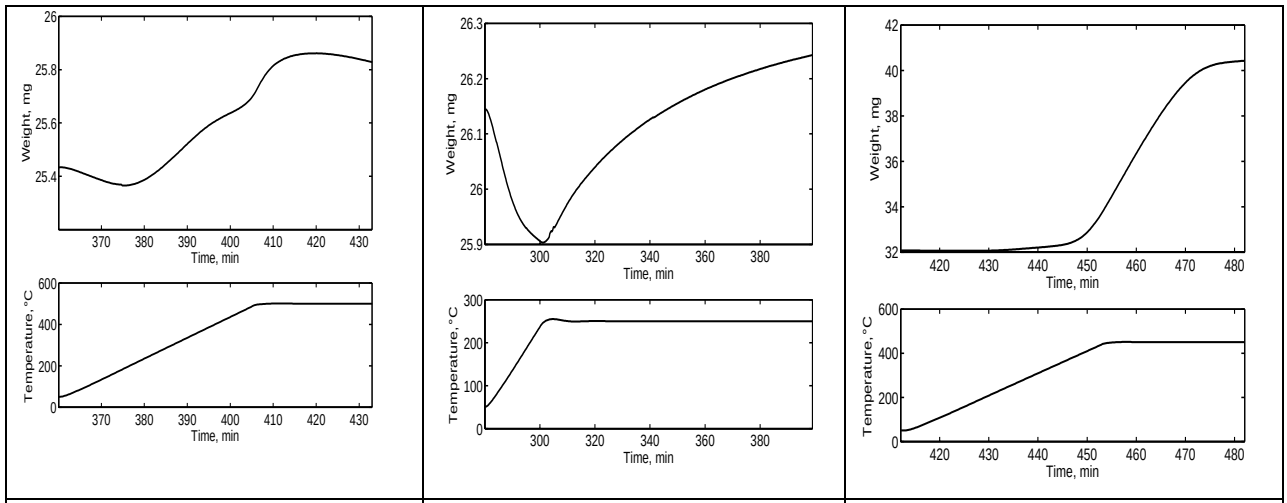

a) Weight loss and temperature profiles for catalyst family A	**b) Weight loss and temperature profiles for catalyst family C**	**c) Weight loss and temperature profiles for catalyst family D**

Figure 37. Results from CO_2 oxidation during TGA-MS screening for the different catalyst families

The final sequence in the TGA-MS screening tests was a reduction with methane. Analysis of the results for this sequence did indicate reactivity for most catalysts. However, interpretation of the results to identify specific product and quantities was more challenging. The only specific reaction that could be easily identified was the coking reaction because of the large weight gain and decrease in gas phase carbon compounds.

In the results presented, there has been no mention of catalyst family B. Catalyst formulations from this catalyst family were tested with the TPR and TGA-MS systems, but the results indicated that these catalysts did not assist in oxygen extraction from CO_2 or enhance hydrocarbon oxidation at lower temperatures.

To overcome the issues with interpretation of TGA-MS data, the bench-scale reactor system was modified to permit testing of the catalysts across a range of temperatures and pressures with methane and other hydrocarbons.

Figure 38 shows the effluent concentrations for CO and H_2 for a sample of Catalyst D. The interesting feature about the effluent concentration in Figure 38 is that the concentrations of H_2 and CO are approximately equal as would be expected from the reaction chemistry.

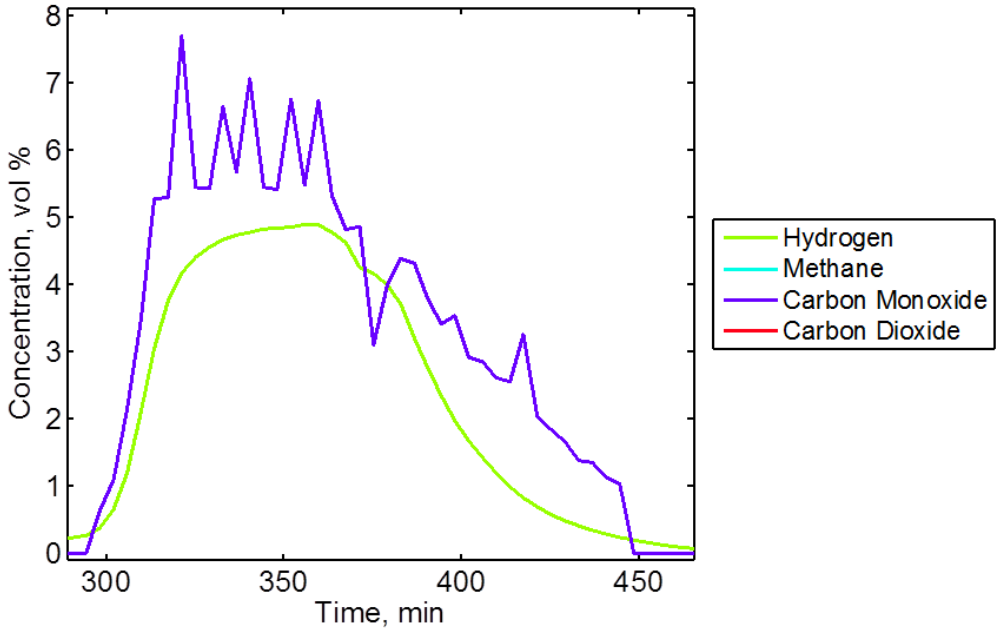

Figure 38. Effluent Concentration Profiles for Catalyst D at 600°C at 25 bar with CH_4 and CO_2

Although the decrease in CO and H_2 might appear to be the result of catalyst deactivation, process conditions were changed to lower the temperature to 400°C and increase pressure from 25 bar to 50 bar. These new operating conditions do not appear favorable for the reaction. The results from a second test conducted at the same original operating conditions as in Figure 38 are shown in Figure 39. These results show the same stoichiometric production of hydrogen and CO with relatively stable effluent concentrations. Unfortunately, the limited duration of both of these tests prohibit demonstration of long term catalyst stability, but the ability to reproduce the result is promising.

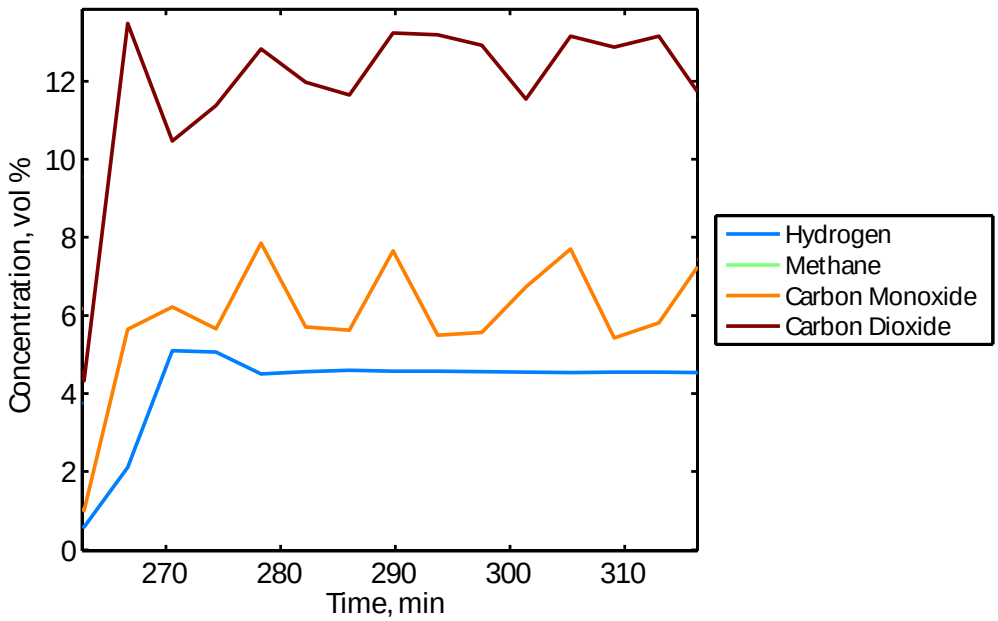

Figure 39. Effluent Concentration Profiles for Catalyst D at 600°C at 25 bar with CH_4 and CO_2

With Catalyst A, analysis of the product gas, shown in Figure 40, indicates the formation of other hydrocarbons specifically ethane and ethylene. These longer chain hydrocarbon products were generated for about 10 minutes during this test. It is interesting that the production of ethylene, ethane and H_2 peak at roughly the same time and subsequently start to decline. The next main product observed is CO, which seems to start to increase at the same time there is a significant decline in ethane production. This would suggest that there are multiple different catalytic sites present on the catalyst and the most active of these are rapidly deactivated.

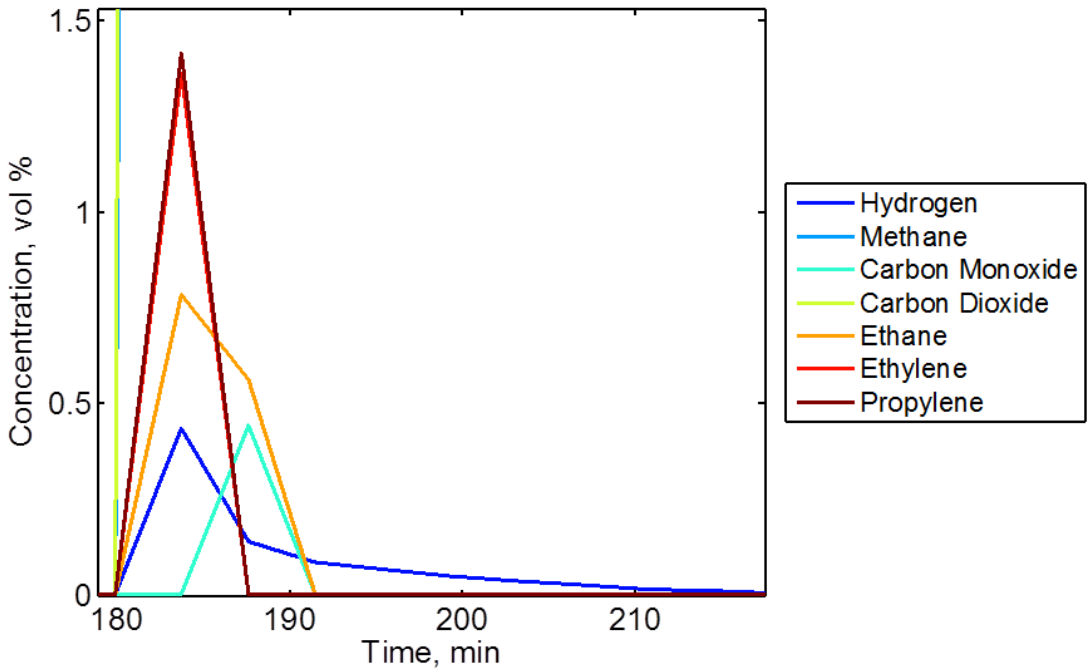

Figure 40. Effluent Product Profile for Catalyst A at 780°C with CH_4 and CO_2

In another test in the bench-scale reactor, Catalyst A was exposed to a reactant mixture of propane and CO_2. The results from this test are shown in Figure 41. The results in Figure 41 show that Catalyst A is able to effectively convert alkanes into alkenes as observed with the production of ethylene and propylene. We believe the mechanism for this transformation uses the oxygen extracted from CO_2 for selective oxidization of the hydrocarbon. Production of ethane, ethylene, and methane also indicates that Catalyst A has the ability to break C—C bonds. The production of alkenes and products from the cleavage of C—C bonds increases to a maximum and drops back to near zero within the first 10 minutes of the test. In this case, this trend is the result of rapid deactivation of these special active sites on the catalyst, because consistent operating conditions are maintained for about 50 minutes after the production of these product species drops back to near zero.

After the deactivation of the catalytic sites that results in conversion of alkanes into alkenes and cleavage of C—C bonds, the composition of the effluent shows relatively consistent production of hydrogen and CO. During this portion of the test, the effluent consists of hydrogen, CO, CO_2, propane, and a small amount of methane. The fact that the same effluent species are observed during testing with methane and CO_2 suggests that reaction mechanism is the same for methane and propane. The absence of any C_2 species in the product during this portion of the test also suggests that reaction mechanism effectively breaks longer carbon chains almost exclusively into C_1 species.

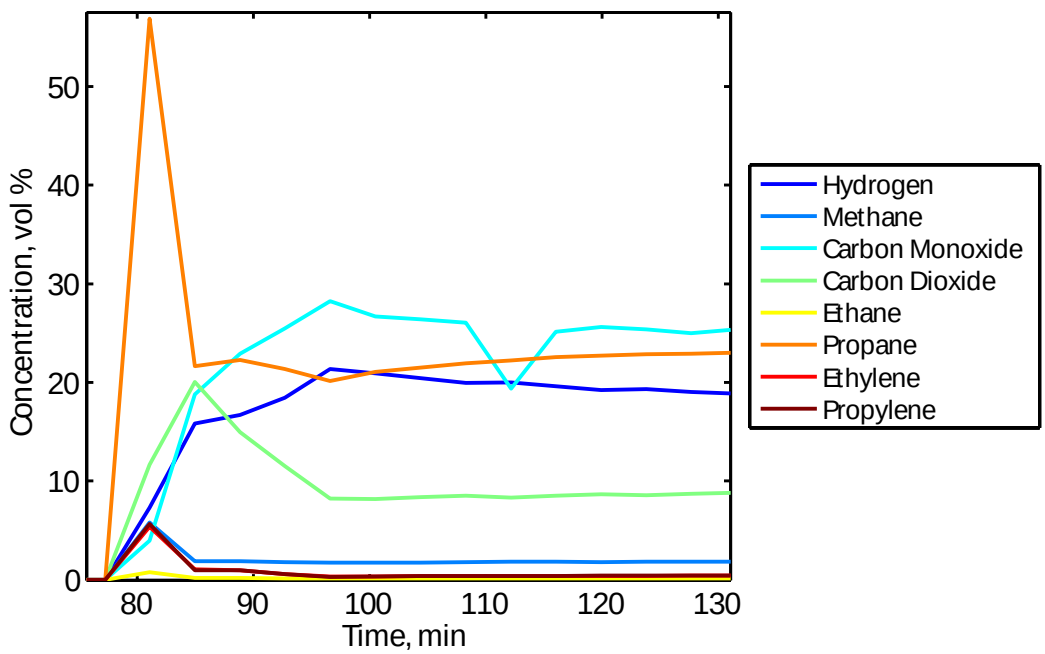

Figure 41. Effluent Product Profile for Catalyst A at 700°C with propane and CO_2

The final observation about the results in Figure 41 is about the transition from the initial reactivity that results in production of alkenes and C—C cleavage to the production of hydrogen and CO. During the production of the alkenes and C—C cleavage products, the alkene and C—C cleavage product effluent concentrations pass through a maximum. By contrast, the effluent concentrations of hydrogen and CO only really begin to increase rapidly after the effluent

concentrations of the alkene and cleavage products begin to decline. These transitions suggest that the reaction mechanism for alkene production and C—C cleavage involves additional/competing reaction steps to the ones required for the production of hydrogen and CO.

The key observations about the reaction mechanism for the production of hydrogen and CO from this testing were (1) it was essentially independent of hydrocarbon feed species, (2) it produced almost exclusively C_1 product species even with feed gas mixtures consisting of longer chain carbon species, (3) it was the dominant reaction mechanism when the most active catalyst sites have been deactivated, and (4) it was either required as part of or competes with the alkene production and C—C cleavage reaction mechanism/reaction steps.

The two most promising research directions for potential products identified during our catalyst screening were carbon chain growth and selective partial oxidation. Although these reaction mechanisms seem to apply generally to alkanes, our subsequent testing focuses on methane because of the abundance of methane available from shale gas and potential simplification of the analysis and interpretation of the products generated. We specifically focused on ethylene production and dry methane reforming.

8.2 Ethylene Production

Our bench-scale reactor system was modified to include a Fourier Transform Infrared (FTIR) spectrometer for product composition analysis. Because of its high sampling frequency, FTIR analysis enables rapid analysis of product gas compositions, which increases the amount of data available on product composition during a short time interval. These data are extremely valuable for analyzing the performance of a catalyst that deactivates rapidly.

The catalyst was loaded in the fixed-bed reactor in its oxidized state and was heated to 800°C in an inert environment at atmospheric pressure. Subsequently, methane gas was introduced into the reactor and the products were analyzed with a FTIR spectrometer. The temperature was ramped at 5°C/min to 900°C and held for 1 hour at 900°C. The ethylene production for the four catalyst families tested are shown in Figure 42. In Figure 42, the introduction of methane and heating start at 100 minutes. At 120 minutes, the reactor temperature is at 900°C.

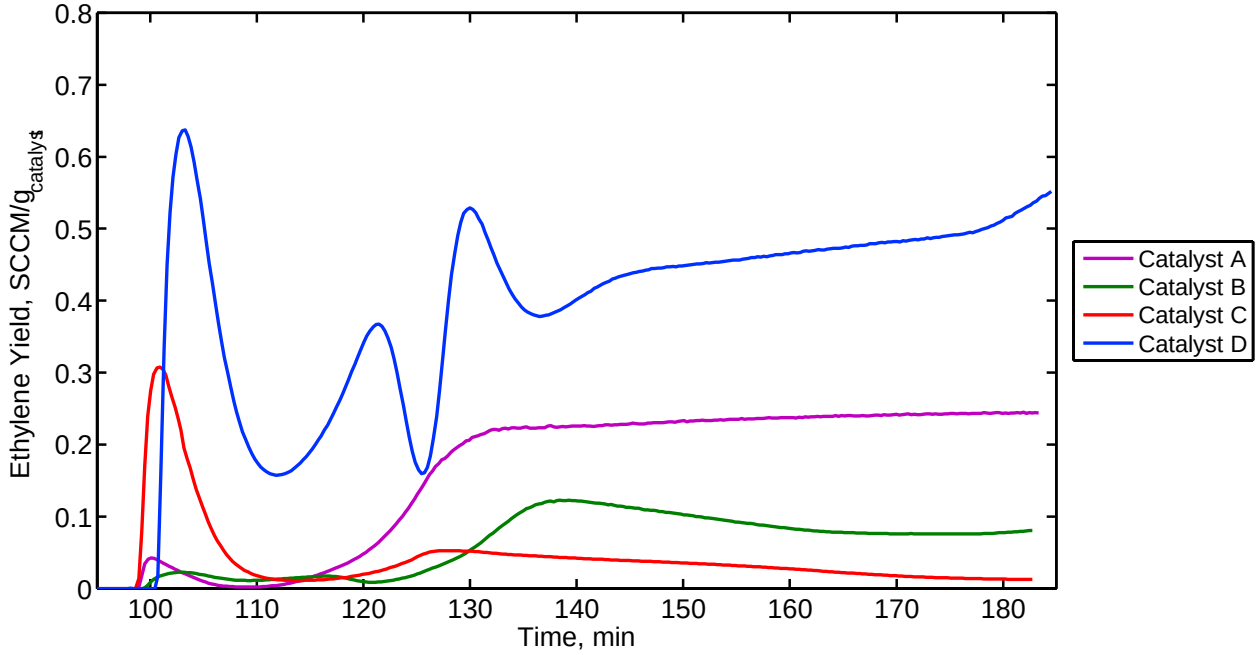

Figure 42. Effluent ethylene yield profiles vs. time for examined catalysts from 800°C to 900°C at atmospheric pressure with a CH_4 feed

The data shows significant differences in the activity of the four different catalysts. Catalyst B shows comparatively lower activity over the full temperature range and does not appear useful. Catalyst A shows moderate activity once the temperature reached 900°C. Catalysts C and D, however, both show higher ethylene yields. Both these catalysts showed the highest levels of ethylene production near 800°C. For Catalyst C, most of the active oxygen sites appeared to be rapidly consumed. After consumption of these most active sites, ethylene production remains very low with only a slight increase as the reaction temperature is increased from 800°C to 900°C. Catalyst D shows more complex and overall higher reactivity than any of the others. There was an initial peak with high ethylene yield, but as reaction temperature reaches 900°C the ethylene yield increases and produces about 0.5 SCCM of ethylene per gram catalyst during the 1 hour hold time. These results hold great potential for further development of a catalyst for the production of ethylene while utilizing CO_2.

8.3 Dry Reforming of Methane

A full factorial of the two process conditions: temperature and CH_4 to CO_2 feed ratio was conducted for each of the four catalyst families at an elevated pressure of 350 psig and 500-600°C. Volumetric production rates of CO and H_2 per mass of catalyst, and the CO to H_2 product ratio were used to evaluate catalyst performance and the optimal process conditions. Regression analysis of the results was utilized to create predictive models for each catalyst depending on the varied factors determined to be statistically significant (95% CI). The models are a function of temperature and the CH_4 to CO_2 feed ratio. Response surfaces were created with the models for each metric and are displayed in Figures 43-45 below.

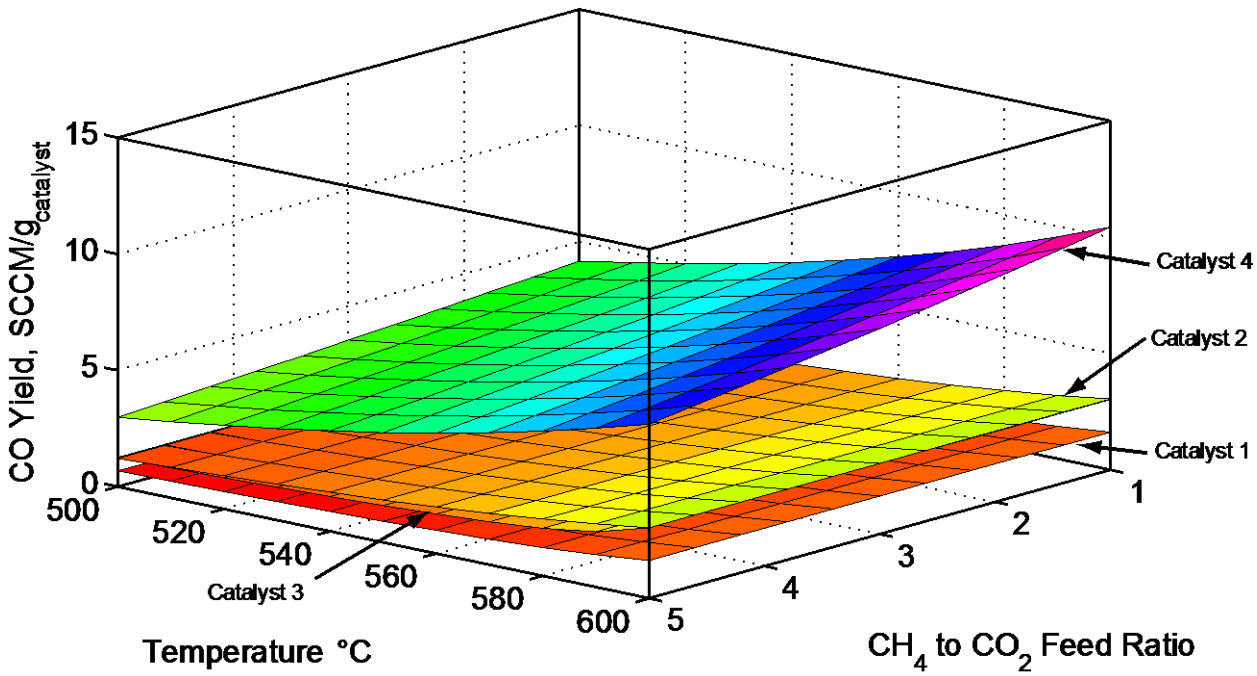

Figure 43. Modeled CO yield response surfaces for different catalysts over varying temperature, pressure, and reactant feed ratios

Figure 43 displays the modeled response surfaces of the four catalysts for the CO yield on a per gram basis. The color scale on the surfaces of Figures 43-45 is representative of the magnitude of each response surface. Each catalyst produced the highest CO yield at a temperature of 600°C and a CH_4 to CO_2 feed ratio of 1. Catalyst 1 had the lowest yield, while the surfaces for Catalysts 2 and 3 are nearly identical, with Catalyst 2 producing a slightly higher yield for most of the operating space. Finally, Catalyst 4 had a much higher yield than the other catalysts, reaching a maximum of 11 SCCM per gram catalyst. Statistical analysis of the results found that improvement of Catalyst 4 compared to the other catalysts was statistically significant. In addition, the lower response of Catalyst 1 was statistically significant compared to the other catalysts. The difference between Catalyst 2 and Catalyst 3 was not found to be statistically significant. These statistical comparisons hold true for the other metrics shown in Figures 44 and 45 as well.

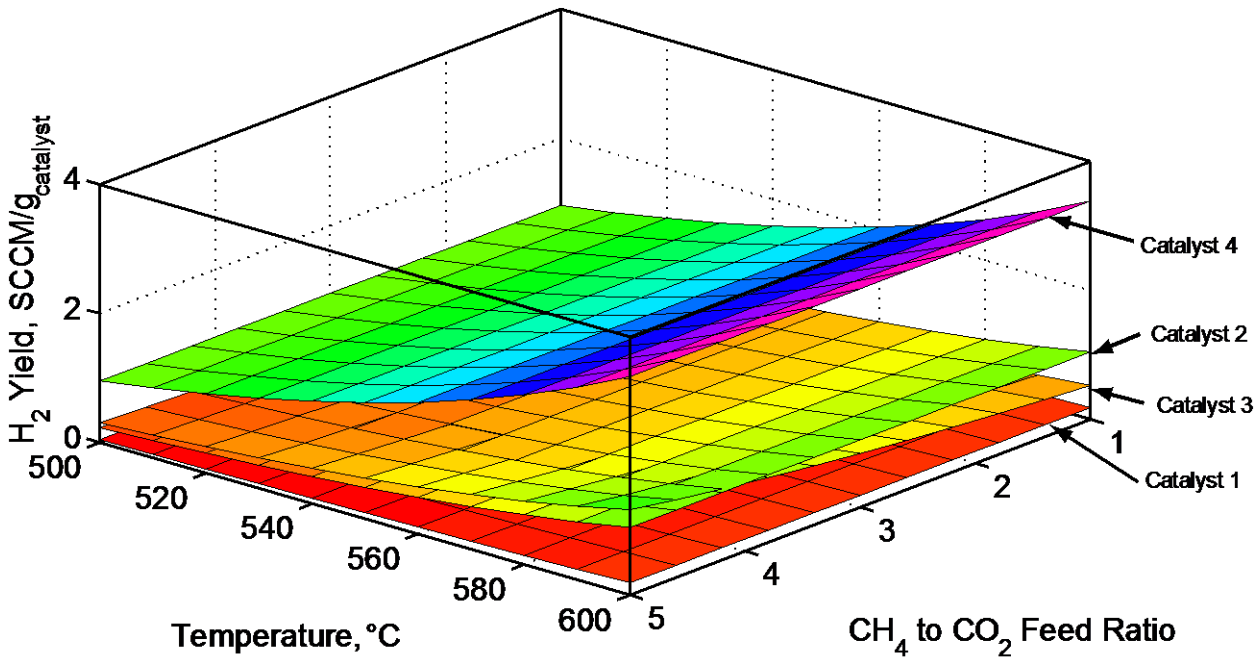

Figure 44. Modeled H_2 yield response surfaces for different catalysts over varying temperature, pressure, and reactant feed ratios

Figure 44 depicts the modeled response surfaces of the four catalysts for the H_2 yield on a per gram basis. The CH_4 to CO_2 feed ratio was only found to be a significant effect for Catalyst 3. The H_2 production of Catalyst 1 was found to be minimal. Catalysts 2 and 3 performed similarly again, however, Catalyst 3 produced a slightly higher H_2 yield at higher CH_4 to CO_2 feed ratios. Catalyst 4 was the best performing catalyst, achieving a maximum yield over 3.5 SCCM per gram catalyst at 600°C.

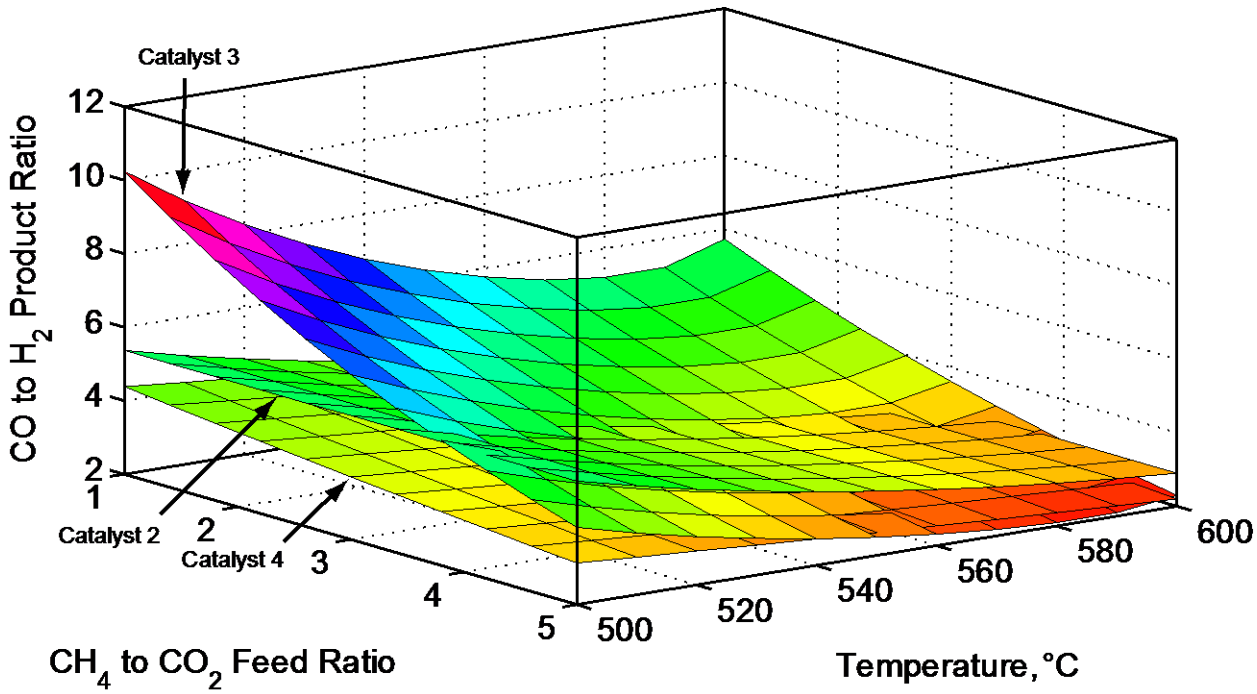

Figure 45. Modeled CO to H_2 product ratio response surfaces for different catalysts over varying temperature, pressure, and reactant feed ratios

Figure 45 shows the modeled response surfaces of the four catalysts for the CO to H_2 product ratio on a per gram basis. Catalyst 1 was not shown in Figure 45, because the low H_2 production resulted in such a high ratio that the other catalyst responses were difficult to discern. The response surfaces in Figure 45 may be used to determine the ideal conditions to achieve various CO to H_2 ratios that different processes may require. In many applications, CO to H_2 ratio near 1 or lower is desired, and Catalyst 4 achieved the lowest ratios near 2:1. Water formation is believed to be the main factor contributing to a CO to H_2 ratio above 1.

These four catalysts have been shown to partially oxidize methane over varying process conditions. Conversion was shown to take place at high system pressures. The best-performing catalyst was identified as Catalyst 4 for each performance metric.

9. Conclusions

In this project, our research has focused on finding reaction chemistry that would permit CO_2 utilization on a scale that could match or exceed our anthropomorphic CO_2 generation caused by our use of fossil fuels for energy. To support achieving this goal, we have found that carbon sources and in particular solid carbon sources can be used as a reductant to convert CO_2 into CO. The most reactive of the carbon sources was biomass and the least reactive were high rank coals and petcoke.

To achieve even higher levels of reactivity and conversion, our efforts turned to catalyst development. Through parametric testing, we were able to systematically refine our catalyst formulations and achieve an increase in reactivity of factor of 70 with petcoke. Through a rather clever use of a naturally occurring isotope of oxygen (O^{18}), we were also able to demonstrate that

our optimal catalyst formulation was able to effectively extract oxygen from CO_2 and use this oxygen to oxidize CO and petcoke.

Because this discovery can effectively enable the use of CO_2 as a selective oxidant for hydrocarbons, this discovery introduces the potential for CO_2 utilization to be conducted on a scale that could match or exceed anthropomorphic CO_2 generation. The power in the utilization of CO_2 as a selective oxidant for hydrocarbons is that it opens up CO_2 utilization for not just one, but multiple reaction chemistries, that could be used to make many (we evaluated 19 in our study) of the most important and largest production volumes commodity chemicals.

With our original work with solid carbon sources and catalyst development for the production of a CO-rich syngas, we were able to complete a preliminary techno-economic analysis for this process and show that it had a promising rate of return on investment. Although our estimation of the premium to be charged for preparation of the carbon source may have been underestimated, even if this premium were increased by a factor of two, the process would still have economic merit.

To begin the work on direct chemical production using CO_2, we investigated the potential for producing ethylene and dry reforming of methane. Several catalysts developed and optimized in this project demonstrated production of ethylene at temperatures between 800°C and 900°C. For dry reforming, a catalyst formulation developed on this project demonstrated reactivity at temperatures between 500°C and 600°C. These results show that with suitable catalysts, CO_2 utilization can be used to produce many of the large volume commodity chemicals currently manufactured.

10. References

Furimsky, E., P. Sears, T. Suzuki, *Energy & Fuels*, **1988**, 2: 634-639

Kajitani, S., N. Suzuki, M. Ashizawa, S. Hara, *Fuel*, **2006**, 85: 163-169.

Kodama, T., A. Aoki, T. Shimizu, Y. Kitayama, S. Kormaneni, *Energy & Fuels*, **1998**, 12: 775-781

Roberts, D. G., et al. *Energy & Fuels*, 14 (2000) 483-489.

Roberts, D. G., D.J. Harris, *Energy & Fuels*, **2012**, 26: 176-184.